LA-3933-MS

LOS ALAMOS SCIENTIFIC LABORATORY
of the
University of California
LOS ALAMOS • NEW MEXICO

Quarterly Status Report on the Advanced Plutonium Fuels Program January 1 to March 31, 1968

UNITED STATES
ATOMIC ENERGY COMMISSION
CONTRACT W-7405-ENG. 36

DISCLAIMER

This LA...MS report presents the status of the LASL Advanced Plutonium Fuels Program. Previous Quarterly Status Reports in this series, all unclassified, are:

LA-3607-MS	LA-3745-MS
LA-3650-MS	LA-3760-MS*
LA-3686-MS	LA-3820-MS
LA-3708-MS*	LA-3880-MS

This report, like other special-purpose documents in the LA...MS series, has not been reviewed or verified for accuracy in the interest of prompt distribution.

*Advanced Reactor Technology (ART) Series

LA-3933-MS
SPECIAL DISTRIBUTION

LOS ALAMOS SCIENTIFIC LABORATORY
of the
University of California
LOS ALAMOS • NEW MEXICO

Report written: April 1968

Report distributed: May 14, 1968

Quarterly Status Report on the Advanced Plutonium Fuels Program January 1 to March 31, 1968

FOREWORD

This is the seventh quarterly report on the Advanced Plutonium Fuels Program conducted at the Los Alamos Scientific Laboratory. In addition to work previously described in this series of reports, the current issue contains the first account of recently initiated studies of solid metallic fuel systems for fast reactors (Project 824).

Most of the investigations discussed here are of the continuing type. The results and conclusions described may therefore be superseded as the program progresses. Published reference to these preliminary results, or quotations of them, should not be made without obtaining explicit permission to do so from the person in charge of the work.

TABLE OF CONTENTS

TABLE OF CONTENTS
(continued)

PROJECT 801

SODIUM TECHNOLOGY

Person in Charge: D. B. Hall
Principal Investigators: G. H. Best
R. H. Perkins

I. INTRODUCTION

High-temperature sodium systems, such as those contemplated for use in fast, central-station-reactor concepts, require a high level of purity control to limit corrosive processes and to preserve reliability. In addition, the advent of large sodium-cooled fast reactors requires a knowledge of fission product release and distribution in the primary coolant system and the development of methods by which this distribution can be altered. To monitor the impurity levels in coolant sodium (and in its associated cover gas system), suitable instrumentation and analytical techniques must be developed. Methods and kinetics of impurity control are studied using these analytical devices as they become available.

The release and distribution of fuel and fission products in sodium systems have been studied using both sealed capsules and forced-convection sodium loops. Preliminary experiments have been performed on the release of fission products from trace-irradiated (U,Pu)C fuel into a sodium column under isothermal conditions and with an axial temperature gradient. Similar experiments have been initiated to study the distribution of individual long-lived gamma-active isotopes in a sealed capsule containing sodium and a potential trapping material.

Long-lived fission products have been introduced into a small, forced-convection sodium loop by immersing a trace-irradiated plutonium alloy in the flowing sodium. The distribution of plutonium, ^{90}Sr, ^{137}Cs, and ^{155}Eu in the loop, over periods of 1000-3000 h, has been observed by *in situ* gamma scanning of loop components and by radiochemical analysis of traps and metal specimens removed from the loop. Hot trapping, cold trapping, and graphite adsorber experiments have been conducted.

The solubility of oxygen in sodium using the vacuum-distillation analytical technique has been determined over the temperature range of 125° to 300°C. An experimental facility to be used for the development of analytical techniques for the measurement of impurities in sodium has been constructed and is being tested. Another sodium loop which will be used in the development of in-line instrumentation and investigation of the soluble gettering technique for impurity control is being built.

The performance characteristics of different designs of cold traps for sodium systems are being determined. Several tests were conducted to determine the rates of change of oxygen concentration in a system following rapid changes in the cold trap temperature. Methods to measure the rate at which gases diffuse into sodium loops have now been tested. Results are encouraging. The fabrication of artificial leaks in sodium containers is continuing. If the program is successful, it may be possible to establish pre-operational testing standards which will insure satisfactory service life for sodium loop components.

II. TRANSPORT AND DISTRIBUTION OF FISSION PRODUCTS IN SODIUM: LOOP EXPERIMENTS (J. C. Clifford)

A. General

The behavior of radioactivity released to

sodium from failed or vented fuel elements may limit access to portions of the primary coolant system and may affect the consequences of a loss-of-coolant incident. Depending on the fission-product release fraction anticipated in either circumstance, it may be desirable to scavenge these species (as well as uranium and plutonium) from the coolant.

The immediate goals of this investigation are: (1) to identify sodium-soluble fission-product species and (2) to examine the effects of primary-coolant-system construction materials, design features, and operating conditions on these species.

B. Current Results

A forced-convection sodium system, assembled to study release and distribution of ^{131}I, ^{140}Ba, ^{137}Cs, and other species from trace-irradiated plutonium fuels,[1] has been operating for purposes of cleanup for 2300 h. Experiments have been delayed by a series of difficulties with the high resolution gamma scanning equipment (section V) associated with the loop.

The "diffusion" cold trap experiment described in an earlier report[2] has been in operation for approximately 8200 h. During most of this quarter (1600 h) the cold trap has been used as an oxygen control device in the study of adsorption of ^{137}Cs on stainless steel surfaces. Specimens of "as-received" and heavily oxidized Type 347 stainless steel, in the form of 2-1/2-in.-wide, 2-mil-thick strips were rolled into bundles and immersed in 225°C sodium containing ^{137}Cs. Spacing between foil layers was provided by winding corrugated and flat sheet together in each bundle. An initial ^{137}Cs activity of 3.6×10^8 dis/min per gram of sodium was provided by dissolving carrier-free $^{137}CsCl$ in sodium at 500°C.

Results from the first experiment show considerable scatter because of several temperature fluctuations in the test section. However, some crude rate estimates were made. At a sodium temperature of 225°C the estimated average rate of pickup of ^{137}Cs activity during the initial 20-h period of the experiment was 6.9×10^5 (dis/min)/(in.^{2}-h) for the "as-received" foil and 4.4×10^5 (dis/min)/(in.^{2}-h) for the oxidized foil. The adsorption of ^{137}Cs was more than 70 per cent complete within 200 h, and no significant changes were detected after 500 h. At the latter time, the activity of the adsorbed ^{137}Cs on "as-received" foils was 1.4×10^7 (dis/min)/(in.^{2}), and that on the oxidized foils was 1.3×10^7 (dis/min)/(in.^{2}).

A reduction in sodium temperature from 225°C to 115°C initiated a reduction in ^{137}Cs activity on the foils. Although the data scatter is significant, the activity loss from both foils appears to be linear with time. These rates of activity loss, averaged over a 200-h period, were 1.4×10^4 (dis/min)/(in.^{2}-h) for the bare foil and 6.4×10^3 (dis/min)/(in.^{2}-h) for the oxidized foil. The presence of a heavily oxidized surface appears to inhibit ^{137}Cs adsorption and to alter the equilibrium partition of activity between the stainless surfaces and sodium. There is some evidence to suggest that the rate of deposition and the initial distribution of cesium also are affected by flow rate.

The loop being used for the adsorption experiments is not suitable for such work because of difficulty in controlling temperatures at low sodium flow rates and because of flow distortions in the test section. The experiments will be transferred to another loop which was put into operation recently. A systematic study will be made of the effects of initial cesium concentration, operating temperature, sodium flow rate, and adsorber surface conditions on the deposition of cesium from sodium solution onto metal surfaces. Stainless steels, nickel-base alloys, and refractory metals will be investigated.

III. TRANSPORT AND DISTRIBUTION OF FISSION PRODUCTS IN SODIUM: CAPSULE EXPERIMENTS
(J. C. Biery, C. R. Cushing)

A. General

The rupture of nuclear reactor fuel elements containing ceramic Pu-U pellets will allow fission products to be leached from the pellets by the sodium coolant. The release rates of these fission products should be known to evaluate sodium system contamination problems. This research program is designed to determine fission product mass transfer rates from ceramic fuel pellets to sodium as a function of temperature, sodium conditions, and pellet composition.

The release of fission products into sodium from irradiated Pu-U ceramic fuel pellets is being

studied by measuring gamma count rate spectra from the pellet and the sodium into which fission products have transferred. The neutron irradiated pellet is enclosed with 3 to 10 in. of sodium in a 12-in.-long capsule. The distribution of fission products as a function of time and position in the capsule is determined by gamma scanning the capsule. The temperatures for the experiments range from 650° to 900°C. The furnace can impose either isothermal conditions or longitudinal temperature gradients up to 25°C/in.

B. Current Results

Two experiments have been run in this report period. The first test was the continuation of the experiment described in the last quarterly report. The conditions of the run were as follows: irradiated (U,Pu)C pellet at 800°C, under 7 in. of sodium, gas/liquid interface temperature of 700°C, 0.244-in.-long x 0.260-in.-diam pellet, 6.7×10^{16} fissions, and 5.5×10^{15} ^{137}Cs atoms. Scans of the capsule were taken 10 and 11 days after exposure to the sodium and measurable amounts of ^{137}Cs, ^{140}Ba-^{140}La, ^{144}Ce, and ^{131}I were detected. Since that time the solid state detector system has been inoperable, and no additional data have been obtained. The experiment was terminated after 95 days at temperature. The outer capsules have been removed in preparation for post-mortem scanning. The capsule will then be sectioned, pellet removed, and sodium again scanned to determine fission product concentrations without the high-level interference of the pellet.

In the second experiment, sodium from an in-pile (U,Pu)C irradiation has been scanned to obtain fission product distributions. The conditions of the irradiation are described in detail under Section VII, Irradiation Testing, in this report. A brief summary of the conditions is as follows: surface temperature of (U,Pu)C pellets, 750°C; sodium temperature, 705° to 750°C; length of sodium column, 2-1/2 in.; diameter of capsule, 0.280 in.; number of pellets, 3; hours of exposure, 113.

The solidified sodium was sectioned into two equal pieces and melted out of the gamma-hot stainless steel fuel cladding. The sodium and stainless steel sections were then counted with a lithium-drifted germanium crystal. A complete identification of the various peaks has not been made. However, the usual sodium soluble fission products (^{131}I, ^{137}Cs, and ^{140}Ba-^{140}La) have been found. Many other peaks have not at present been identified. With the sodium in direct contact with the (U,Pu)C pellets during irradiation, fission products normally not seen in the sodium in out-of-pile experiments would show up because of direct extraction of short-lived precursors and the surface knock-off of fuel material by fission fragments. A comparison of the results from the two experiments described here may give some indication of the importance of the short-lived precursors in fission product transfer from the (U,Pu)C pellets.

IV. GAMMA RAY SPECTROMETRY
(J. C. Clifford, R. Wilhelm)

A. General

The routine identification of individual gamma emitters in a spectrum of mixed fission products requires a gamma spectrometer of high resolution, an automatic data handling system, and well-defined, reproducible counting geometries. While single components, such as ^{137}Cs, have been assayed using sodium iodide detectors and scalers, simultaneous investigation of several isotopes (^{131}I, ^{140}Ba-^{140}La, ^{95}Zr-^{95}Nb, ^{144}Ce, and ^{106}Ru-^{106}Rh) has been postponed while suitable equipment and techniques are developed.

B. Current Results

Operation of the semiconductor anticoincidence gamma scanning system has been delayed further by a series of problems with the scanner drive, the detector cryostat, and with the detector itself. The mechanical, electronic, and vacuum difficulties have been resolved, but the detector has been returned to the vendor. There has been no indication of when a suitable detector will be available.

V. TRANSPORT OF STRUCTURAL, CONTAINER, AND GETTER MATERIALS IN SODIUM
(J. C. Biery, C. R. Cushing)

A. General

Fission product gettering studies have indicated that the use of carbon beds in a sodium system may be useful for ^{137}Cs removal. Carbon, however, is slightly soluble in sodium and can carburize austenitic stainless steels and refractory metals.

The temperature dependence of this rate process is not known. Therefore, the purpose of this study is to determine the temperature range in which the carbon mass transfer rates are sufficiently low to allow use of carbon beds in a sodium system.

The carbon transfer rates from carbon rods will be studied in thermal convection loops. The Type 304 or 316 stainless steel loop itself will serve as the carbon sink when these materials are studied. In a second series of runs, vanadium alloy sleeves will serve as the getters.

B. Current Results

All but one of the parts for the thermal convection loop have been received, and assembly will soon be started. The containment for the loop is complete, and the instrumentation for the loop has been assembled.

A literature survey on carbon mass transfer was completed. No references could be found where elemental carbon was the source and stainless steel was the sink. The survey indicated, however, that carbon activity is greatly influenced by the oxygen activity in the sodium. This observation dictates that the mass transfer runs be made with both high (25-50 ppm) and low (< 5 ppm) oxygen concentrations.

Vanadium alloys have been ordered for testing in the thermal convection loop.

VI. SAMPLING AND ANALYTICAL TECHNIQUES
(V. J. Rutkauskas, G. E. Meadows, K. S. Bergstresser)

A. General

Dynamic in-line sodium sampling techniques for the vacuum distillation analytical method are presently being evaluated. The objective of this phase of the program is to develop a prototype sampling system for engineering systems and reactor plant application. To complement this study, alternate techniques will be developed and evaluated. Although the vacuum distillation method has many advantages over the more widely accepted techniques for impurity analysis in sodium and has demonstrated reliable oxygen analyses on sodium typical of reactor coolants, there are a number of problem areas which must be investigated to assess the over-all capabilities of the method. Of prime importance are the nature of the residues following a distillation and the effects of distillation temperatures on the nature of the residues.

The (γ,n) activation technique for the determination of carbon and oxygen in sodium has the capability for measuring oxygen specifically rather than relating the oxygen content to total alkalinity or sodium content. This method is theoretically capable of determining the concentrations of these elements directly with a sensitivity of < .1 ppm. It should provide a standard for evaluating other methods for oxygen analysis.

The development of prototype in-line analytical instrumentation for the continuous monitoring of oxygen and/or metallic impurities of interest in sodium systems is a basic requirement for the *in situ* characterization of large-scale sodium systems. In-line impurity monitoring devices measure a characteristic or property of sodium that is sensitive to impurity concentrations present in the flowing stream. The United Nuclear Corporation electrolytic cell oxygen meter and the LASL dc electrical resistivity meter concept, which is still in its formative design stage, have both shown a tremendous potential for the in-line analytical capability in sodium systems during the course of their respective preliminary testing. These analytical techniques must be rigorously evaluated over a range of impurity concentrations, flow, and temperature conditions in order to fully evaluate their capabilities and limitations.

B. Current Results

A continuing effort is being applied to the design of a remotely operated full-flow vacuum distillation sampling system for the radioactive sodium chemistry loop in the EBR-II. A manually operated version of this sampling system is also being developed for installation in the nonradioactive secondary sodium system of EBR-II. As presently envisioned, the sampling system will be an engineering loop version of the laboratory model full-flow vacuum distillation sampling system presently being operated on the Analytical Loop No. 1 and Cold Trap Experimental Facilities. The sampling system will be all metal and the separation of the sodium from the nonvolatile impurities will be accomplished with an induction generator heat source. The work coil of the induction generator will be located within

the metal envelope. The sample variance obtained with the full-flow sampling system has been ± 0.1 g as compared to ± 10% with the integral vacuum distillation sampling system for the same sample cup volume (5 g).

Fabrication of the sodium shear and extruder mechanism has been completed. Following final assembly and preliminary operational check-out, this equipment will be used in the program to evaluate the (γ,n) activation technique for oxygen and carbon in sodium. The electronic equipment needed for the remote operation of this experiment is undergoing preliminary check-out procedures.

Preliminary assembly of the Sodium Analytical Methods Facility has been completed and final assembly has been initiated. The preliminary assembly was conducted to insure the proper alignment and leak tightness of the various components which comprise the facility. In addition, this provided an oportunity to make an operational check on the various mechanisms prior to the final assembly. This facility will be used initially to develop analytical methods for the determination of microconcentrations (1-10 ppm) of carbon in sodium. After the completion of this program, it will be used to study the interactions of dissolved impurities in sodium and to identify the residues which remain following the distillation separation of sodium.

A vacuum inert-gas glovebox facility, which was received during the reporting quarter, has been installed and is presently operational. Modifications to the vacuum system and inert gas recirculation system were necessary to provide the required reliability and flexibility of operation. The acquisition of this facility will greatly reduce the atmospheric contamination normally encountered in handling alkali metal samples; therefore, it will provide additional freedom in the program to develop sampling and analytical techniques.

VII. SOLUTION GETTERING
(V. J. Rutkauskas, R. R. Derusseau)

A. General

For future large sodium-cooled reactor systems, it may be desirable to use soluble getters for control of oxygen and other dissolved impurities in lieu of the more conventional hot and cold trapping techniques. The soluble metal getters of interest either occur in the sodium coolant naturally (calcium and barium), or are produced during reactor operation (as with magnesium). The techniques for the controlled additions of these getters, maintenance of fixed getter levels, and the selective removal of depleted getter metals and other impurities from dynamic sodium systems must be developed. The significant chemical reactions occurring in a sodium system containing these soluble getters must be understood and controlled. This mode of quality control using a soluble getter has the potential for effectively controlling not only oxygen, but also carbon, hydrogen, nitrogen, and possibly metallic impurities.

B. Current Results

Assembly of the Analytical Loop No. 2 experimental facility, which will be used for solution gettering studies and for development and evaluation of prototype on-stream analytical instrumentation, is approximately 80% completed. The large volume sodium reservoir, main pump loop, and two of the three small loop circuits have been installed. In addition, the instrumentation and control circuitry are finished, and the installed portion of the system has been insulated.

VIII. KINETICS OF SODIUM COLD TRAPS
(C. C. McPheeters, J. C. Biery)

A. General

Proper design of an adequate sodium system cold trap for removal of oxygen requires a knowledge of the mechanisms of sodium monoxide precipitation and the mass transfer coefficients as a function of temperature, sodium flow characteristics, and the cold trap geometry. The purpose of this study is to determine the effect of the above variables on the over-all mass transfer coefficient of oxygen in sodium. Mass transfer coefficients can be calculated from oxygen removal rate data when the precipitation surface area and temperature gradient in the cold trap are known. Although the temperature profile can easily be measured, the nature and extent of the surface area must be estimated. An area equivalent to that of the bare cold trap was used in the model, and the assumption was made that the character of the surface did not change appreciably during growth of Na_2O crystals.

Cold trapping tests were conducted in a 60-gal sodium system equipped with a distillation sampler, a plugging meter, and two UNC (United Nuclear Corporation) oxygen meters for oxygen determination. The cold trap testing procedure included an equilibration period at the initial cold trap temperature followed by a rapid change in temperature and the measurement of oxygen concentration at short time intervals.

B. Current Results

Experimental work with Cold Trap No. 1 was concluded during this reporting period. Oxygen concentration transients were performed for oxide additions and oxide removal from the sodium. Concentration was measured as a function of the number of system turnovers, and the oxide removal and addition rates were used to calculate mass transfer coefficients at various cold trap temperatures and sodium flow velocities. The experimental data were simulated by numerical and analytical calculation techniques.

The computer simulation allows the use of nonlinear temperature and saturation concentration profiles, slug flow delay times, and different mass transfer coefficients for precipitation and dissolution of Na_2O. This mathematical model serves three purposes: (1) Since it can simulate the experimental data more closely than simplified analytical models, it produces a standard against which the results from the analytical models can be compared. (2) It can produce a refined set of rate parameters from the cold trap data. (3) It can, when the rate parameters are known, predict realistically the oxygen removal characteristics of a cold trap in a given system.

The first program uses the Lagrangian point of view in which an element of fluid is followed around the system. The element gives up or picks up oxygen in the cold trap; it is moved through the pipes in slug flow fashion, and it is mixed with other elements in the storage tank. In the cold trap, the element is assumed to move as a disk of fluid and to have a uniform concentration at each indexed position. Oxygen is lost to or picked up from the walls as indicated by Eq. 1.

$$\Delta m = k\, \Delta A (C - C_e)\, \Delta t \qquad (1)$$

Δm = mass of oxygen transferred in Δt, k = rate constant (or mass transfer coefficient), ΔA = area of contact with wall, C = average concentration in element of fluid, C_e = saturation concentration at wall, and Δt = time required for element to flow past area ΔA. k assumes different values depending upon the sign of $(C - C_e)$.

With this program, sodium oxide can initially precipitate at high system concentrations and then redissolve when the system concentration decreases. In later stages of runs, when the system concentration is low, mass is redistributed in the cold trap.

A supplementary program has been written to allow for two dimensional variations of concentration in the cold trap and for radial variation of velocity. This program gives an indication of the degree of cross flow in the trap and the variation of k with flow rate when the mass transfer is diffusion limited.

The effect of temperature and flow rate on the mass transfer coefficient, k, is shown by the Arrhenius plots in Fig. 1. The solid lines are drawn

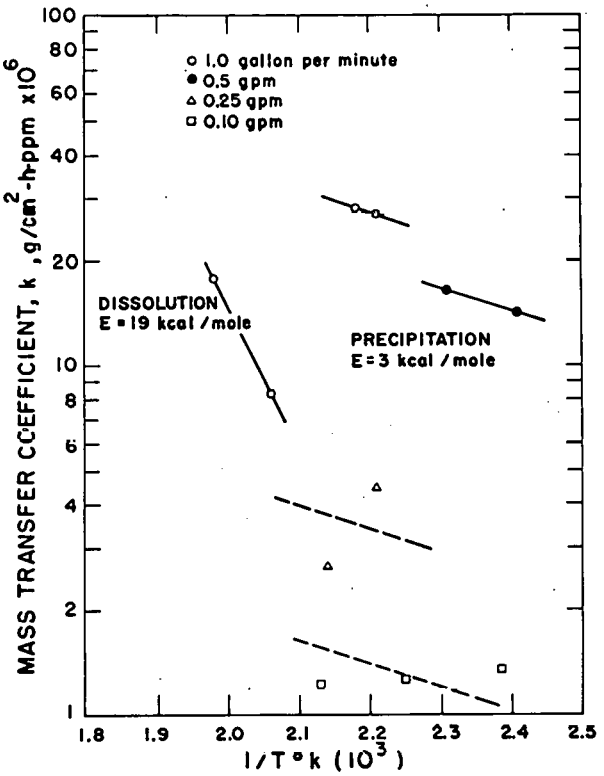

Fig. 1. Arrhenius plots of mass transfer coefficients at various sodium flow velocities. Data from experimental Cold Trap No. 1.

through data points from cold trap runs which are in excellent agreement with the theoretical model. The dashed lines represent the probable slope of the curve for the low flow rate data, which fit the theoretical model very poorly. Sodium entering the cold trap during the low flow rate runs underwent a very sudden drop in temperature to a level well below the saturation temperature. This rapid change in temperature probably led to nucleation of oxide crystals in the liquid phase. The theoretical model was based on the assumption that only surface nucleation and growth occurs. The small crystals suspended in the sodium would then be carried back into the system to redissolve and cause a low apparent mass transfer coefficient. The 1.0 and 0.5 gpm (1.24 and 0.62 cm/sec) runs were done with a shallow temperature gradient, and under these conditions, most of the oxide present in the sodium could diffuse to cool surfaces to nucleate and grow in a lower energy form. In these cases, liquid phase nucleation, if present, was less significant.

The activation energy for precipitation of sodium monoxide from sodium is 3 kcal/mole. This is in good agreement with the reported activation energy for diffusion of sodium monoxide in sodium of 2.4 kcal/mole.[3] The increase in the mass transfer coefficient with increasing sodium velocity, plus the agreement with diffusion activation energy, indicates that the precipitation process is diffusion-limited. Precipitation-rate-limited mass transfer should be much greater.

The activation energy for dissolution of sodium monoxide in sodium is 19 kcal/mole. This high activation energy shows that the dissolution process in this case is not diffusion-limited. The difference between the dissolution activation energy and the precipitation activation energy is equal to the heat of solution of sodium monoxide in sodium. The heat of solution determined from the LASL oxygen solubility curve is 16 kcal/mole. Note that the precipitation activation energy determined here is actually a diffusion activation energy; however, it can be concluded that the dissolution activation energy must be greater than 16 kcal/mole since a negative activation energy for precipitation is not possible. Therefore, 19 kcal/mole activation energy for dissolution seems reasonable.

A further observation can be made concerning the probable value of the precipitation-rate-limited mass transfer coefficient. Consider the following chemical equation

$$Na_2O(c) \rightleftarrows Na_2O \text{ (in solution in Na)}. \qquad (2)$$

The equilibrium constant for this reaction is given by

$$K = \frac{k_d}{k_p} \simeq C_s \qquad (3)$$

where

K = equilibrium constant
k_d = dissolution rate constant
k_p = precipitation rate constant
C_s = concentration of Na_2O in solution in Na

At 200°C, C_s is 12.5×10^{-6} mole fraction. Also at 200°C, k_d was measured as approximately 5.2×10^{-6} g/cm^2-h-ppm. Therefore, the true precipitation rate constant at 200°C should be approximately 0.4 g/cm^2-h-ppm. This value is over four orders of magnitude greater than the measured diffusion-limited rate constants. Experiments in which the rate of oxide precipitation in high velocity sodium was observed (work with plugging indicators described elsewhere in this report) resulted in mass transfer coefficients in the range of 0.1 g/cm^2-h-ppm. This value is nearer to, but still somewhat smaller than, the theoretical rate constant.

From these preliminary results, it is apparent that high velocity cold traps may result in higher oxide removal rates; however, the mechanical strength of the oxide will probably limit the maximum practical sodium velocity which may be used without reentraining precipitated oxide.

IX. PLUGGING INDICATORS
(C. C. McPheeters, J. C. Biery)

A. General

It has been customary to interpret Na_2O plugging temperatures as Na_2O saturation temperatures.[4] However, when plugging indicator temperatures are compared to the latest solubility curves they are lower than the corresponding saturation temperature for a given oxygen concentration.[5,6,7,8,9] The reasons for this divergence in temperature are: (1) the precipitation process in the orifice of a plugging indicator is a rate process and requires finite concentration driving forces to precipitate the Na_2O

in a finite time; and (2) on a bare orifice, a concentration difference is required to initiate precipitation. This rate process at one orifice opening can be expressed as follows:

$$\frac{dm}{dt} = kA_p(C - C_s). \quad (4)$$

m = mass of Na_2O precipitated, g; t = time, minutes; k = precipitation constant, grams of Na_2O/cm^2-ppm-min; A_p = precipitation area on wall of hole, cm^2; C = concentration of oxygen in bulk stream, ppm; and C_s = saturation concentration at orifice temperature, ppm.

For most plugging runs, the cooling curve can be approximated by a linear temperature function or a series of connected linear curves. In the first case, $(C - C_s)$ is equal to $(R_cSt + \Delta C)$ where R_c is the cooling rate (°C/min), ΔC is the concentration difference required to initiate precipitation, and S is the slope of the solubility curve over the concentration range of interest. With this substitution, Eq. 4 can be integrated to give Eq. 5, which also includes the orifice flow equation.

$$k = \frac{r_o(\frac{\Delta G}{G_o})\ \rho(Na_2O)}{R_c\ S\ t^2 + 2\ \Delta C\ t} \quad (5)$$

In (5), t = time to plugging after precipitation is initiated, min; $\rho(Na_2O)$ = density of Na_2O precipitate, g/cm^3; r_o = radius of orifice, cm; and $(\Delta G/G_o)$ - fractional flow change.

B. Current Results

Plugging Runs with a Bare Orifice

Both k and ΔC are functions of the flow and temperature conditions of the sodium passing through the orifice. Many plugging runs have been analyzed to determine the dependence of k upon flow rate, temperature, and concentration and the dependence of ΔC on flow rate, cooling rate, and concentration.

The data collected to date indicate that k is a function of flow rate. The dependence appears to be exponential with velocity; the value of the exponent is between 0.5 and 0.8. Velocities between 50 and 500 cm/sec have been studied and k values between 5×10^{-3} to 1.5×10^{-1} g of O/(ppm-h-cm^2) have been observed. The high values apparently result from the increased area due to fast nucleation and growth of the oxide precipitate.

The model postulated in Eq. 5 assumes that a dense cylindrical layer of Na_2O is precipitated on the inside surface of the orifice. Under conditions of small concentration differences, this condition is probably approached. However, with large concentration differentials many nuclei are precipitated almost simultaneously, and the apparent k constants are greatly increased. This change in kinetic behavior probably indicates that the orifice cylindrical surface is covered by small particulate oxide crystals which present a much larger precipitation area than is indicated by the annular layer mode.

The time to nucleation of oxide on the orifice depends upon the concentration difference required to initiate precipitation (ΔC). The time to nucleation varies from hours with ΔC less than a ppm to a few minutes with ΔC in the 5 ppm or greater range. Therefore, to keep ΔC small in a normal plugging run with a bare orifice, the cooling rate should be very slow. With a slow cooling rate, sufficient time is allowed for nucleation of the oxide with a small ΔC. It is apparent that the cooling rate of the orifice greatly influences the degree of temperature depression that occurs before precipitation starts. With cooling rates greater than 20°C per minute, temperature depressions of 30°-50°C have been observed.[8] The Russians have reported similar effects.[9,10] In the present work, temperatures have been oscillated about a 220°C saturation temperature by ± 30°C with no precipitation observed on the bare orifice.

Plugging Runs with a Partially Plugged Orifice

Once the plug has started to form on the orifice, nucleation effects are no longer important and Na_2O is transferred to and from the orifice as indicated by Eq. 4. Thus, the equilibrium saturation temperature can be determined by oscillating the plugging meter temperature and observing temperatures at the maxima and minima in the flow curve. The temperature must be kept in bounds so that the plug will neither completely dissolve nor completely block the orifice. This principle of determining plugging temperatures with a partially plugged orifice has been utilized by the French (1963)[11] and the British (1966)[12] in meters which continuously determine the equilibrium saturation temperatures.

In the present studies, it was discovered that

a standard plugging indicator could easily be modified to give continuous oscillating temperature and flow traces by installing an off-on control on the cooling blower. The blower is turned on automatically when the flow exceeds a desired set point and is turned off when the flow falls below the set point. The saturation temperature is then determined at each maximum and minimum in the flow curve. With a freshly formed plug and a saturation temperature near 220°C (16.6 ppm),[5] a maximum or minimum will occur every two minutes. At 107°C (1.3 ppm)[5] the kinetics are very slow because of the small concentration differences, and a maximum or minimum will occur every 10 to 20 minutes.

The "oscillating plugging indicator" was tested at cold trap temperatures which ranged from 225°C to 107°C. Satisfactory operation was found over this complete range. The saturation temperature recorded by the continuous plugging meter was within ± 1°C of the equilibrium cold trap temperature. Any one temperature obtained from one maximum or minimum was within ± 2°C of the saturation temperature. An average of 4 to 5 such temperatures was less than ± 1°C from the saturation temperature.

Change in Kinetics of Na_2O Plug with Time

As indicated above, the apparent kinetics of a given oxide plug are affected by the initial concentration driving force. In addition, after many cycles the rates of plug dissolution and growth becomes much slower. This behavior results in a continued decrease in flow oscillation amplitude for a given temperature amplitude. The apparent k constants for dissolution and precipitation decrease by as much as a factor of 10 in this period. Possibly, a recrystallization of the plug occurs, and less surface area is available for precipitation and dissolution. With the reforming of the plug, the Na_2O may take the shape of the cylinder postulated in Eq. 5.

Stability of On-Off Control Mode for "Oscillating Plugging Indicator"

The cyclic behavior of the "oscillating plugging indicator" in early tests was, in general, stable. However, when a new plug was formed, the kinetics were sufficiently rapid to produce oscillations with increasing amplitude. To obtain stability, the flow through the orifice was decreased to slow the kinetics of precipitation and dissolution. Stability was achieved when the heating and cooling rates of the plugging indicator were more rapid than the growth characteristics of the plug. Since the kinetics naturally became slower with time as the plug reformed, the oscillating behavior became more stable.

Dissolution Rate Constants

Equation 5 can be used to generate k constants for the dissolution of the oxide at temperatures above the saturation temperature. ΔC for nucleation does not apply in this case and is given a value of zero. Again, the calculated rate constants are only apparent and are, in general, much higher than the real rate constants. The main reason for the large observed constants is that, as dissolution occurs, small particles of oxide can be eroded from the orifice by the flowing sodium. With a rapidly precipitated plug, rate constants as high as 3×10^{-1} g O/(ppm-h-cm^2) have been observed. However, as the plug ages, the rate constants decrease. As the plug recrystallizes, the area exposed to sodium decreases. With the formation of larger crystals in the orifice, the possibility of particulate erosion also decreases. Constants as low as 1×10^{-3} have been observed with a well aged plug.

X. BASIC STUDIES

1. Correlation of Sodium and Helium Leak Rates (D. C. Kirkpatrick, J. P. Brainard)

A. General

The correlation of sodium leak development with measured helium leak rates provides information on the degree of component integrity which must be attained for safe long-term sodium plant operation. No firm criteria now exist that establish acceptable levels of tightness for various situations.

This study uses fabricated stainless steel leaks and leaks that occur naturally in stainless steel bar stock. Leaks having different helium leak rates will be incorporated into small sodium systems (cells) which will be held at a predetermined temperature until sodium leakage occurs.

B. Current Results

The equipment setup for the first experiment is shown in Fig. 2. The sodium cells are behind

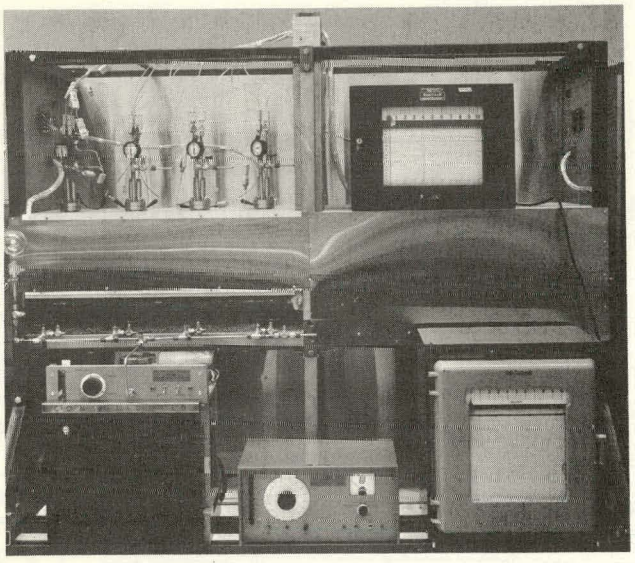

Fig. 2. Apparatus for first sodium-helium leak correlation experiment. Leaks are connected to four sodium cells. The cells will be run at about 450°C until sodium leakage is detected on the mass spectrometer. The cells are located behind the left-hand metal panel, and the mass spectrometer is at the lower left, with a power source next to it. The upper recorder is for the temperatures of the sodium cells, and the lower recorder is for the output from the mass spectrometer.

the left-hand metal panel. The mass spectrometer (lower left in figure) will be continuously calibrated during the experiment.

Four cells will be tested initially: a cell with a compressed tube having a helium leak rate of 1.1×10^{-4} atm-cm^3/sec and its control with no detectable leak, and a cell with a porosity leak of 1.7×10^{-4} atm-cm^3/sec and its control with no detectable leak. These leaks and controls have been thermally cycled and found to be stable. Although these leaks are large, a drop of water will mask them completely; they can be reopened upon vacuum firing.

Sodium transfer capsules were filled with sodium and radiographed to check that they were properly filled. Before sodium is introduced into the cells, the leak system will be brought up to temperature (about 450°C) with only helium in the cells. The leak rates will be studied as temperature is increased. The sodium will then be introduced.

2. Diffusion of Gases in Metals
(J. P. Brainard)

A. General

Very little quantitative information is available on the diffusion of gases in reactor system containment materials, although this phenomenon is known to occur in high-temperature liquid-metal-cooled systems. By use of ultra-high vacuum techniques and a mass spectrometer residual gas analyzer, diffusion rates of 1×10^{-11} to 1×10^{-12} torr-liter/sec-cm^2 (about 1×10^{-14} to 1×10^{-15} g/sec) equivalent nitrogen should be easily observable by means of a pressure change in a fixed volume.

B. Current Results

The initial permeation experiment design is shown schematically in Fig. 3. The first diffusing

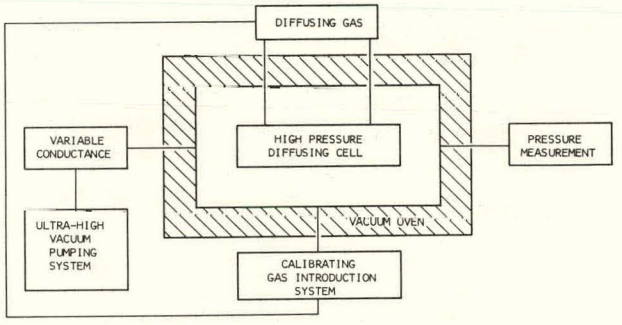

Fig. 3. Experimental arrangement for gas permeation. The diffusing cell contains the gas studied at atmospheric pressure. The gas permeating through the cell is determined by the vacuum pressure. The variable conductance controls the pumping speed of the system in order to keep the pressures within the range of the gauge. The calibrating gas introduction system correlates pressure changes with flow.

cell used will be a Type 304 stainless steel tube with two-mil wall in the form of a coil. Permeation rates are determined by the steady state flow obtained through the metal. The tube will be baked in ultra-high vacuum before the gas of interest is introduced. The time to steady state is proportional to the square of the wall thickness. A two-mil wall iron tube at 400°C with an atmosphere of nitrogen pressure on one side would take over a week to reach steady state flow. Two-mil walled tubes are believed to be the thinnest which can be obtained in stainless steel with a wall variation within ± 10%.

A mass spectrometer will be used for the pressure measurement for unambiguous results.[13]

Thermal desorption spectra, obtained by resistance heating of the tubing, should reveal the

mechanism of gas adsorption and desorption.

The mass spectrometer will be continuously calibrated by periodically introducing a known flow (leak) of the gas of interest. Calibrated leaks of many gases have recently become commercially available. These leaks will greatly simplify the method of calibration.

The initial permeation experiment was designed to determine a wide range of gas diffusion and permeation rates at various temperatures. Subsequent experiments will allow variation of the diffusing cell geometry, the type of metal, and the wall thickness.

XI. COVER GAS ANALYSIS
(C. R. Winkelman, J. P. Brainard)

A. General

Cover gas analyzers for high-temperature sodium-cooled reactors must be capable of detecting impurities such as nitrogen, oxygen, hydrogen, carbon dioxide, and methane in the cover gas with a sensitivity adequate to measure these impurities from the part-per-million range to the per cent range. The analyses should be accurate to at least 5% and reproducible to about 1%. High-temperature on-line operation would be necessary to prevent adsorption of sodium compounds and fission products on the walls of the apparatus.

A prototype analysis system has been constructed with which to investigate the special needs of 500°-600°C cover gas analysis apparatus. The prototype includes a wide-range bakeable quadrupole mass filter residual gas analyzer. Design techniques used in the prototype are representative of those required for a 500°-600°C system.

B. Current Results

Library research on mass spectrometers operating at elevated temperature has provided possible methods of compensating for temperature effects in the gas analysis.[14,15,16] The changes in measurement sensitivity with temperature can be corrected by using an inert gas of known concentration as a reference in the gas sample. Since the ionization cross section of the inert gas is nearly independent of temperature up to 1000°C, any change in its mass peak height must be due to temperature-dependent changes in instrument sensitivity. The sum of the mass spectrum of a gas with fixed concentration is constant with temperature if normalized by the inert reference gas. This method not only removes sensitivity variations, but also compensates for cracking pattern variations with temperature.[14] It is ideal for inert cover gas analysis since the inert-gas reference is already present.

A dynamic gas mixing system recently received allows us to change the dosing rates and thus the impurity level of a carrier gas by dialing a knob. The system is capable of mixing two impurity gases in a carrier gas from ppb to per cent levels in 10% intervals within decade steps. Manifolds were designed and partially built for an initial gas mixture of nitrogen with helium impurity, and a design to interface this instrument with the cover gas analyzer was completed. With the gas mixing system, we can investigate the following characteristics of the cover gas analyzer:

1. Linearity of analysis with impurity level and carrier gas,
2. Minimum detectable contamination, and
3. Temperature effects on the mass spectrum.

The dynamic gas mixing system has disclosed nonlinearities in the analysis of gas contaminants below 500 ppm. Elution is believed to be the source of these nonlinearities; i.e., gas adsorbed on the analyzer walls is mechanically bumped off when the gas sample is introduced. A new introduction system has been designed and constructed which will minimize elution effects and will make high temperature sampling possible.

REFERENCES

1. J. C. Clifford, "Quarterly Status Report on the Advanced Plutonium Fuels Program," October 1 - December 31, 1967, Report LA-3880-MS, Los Alamos Scientific Laboratory, p. 6.
2. J. C. Clifford, "Quarterly Status Report on the Advanced Plutonium Fuels Program," July 1 - September 30, 1967, Report LA-3820-MS, Los Alamos Scientific Laboratory, p. 6.
3. S. Siegel and L. F. Epstein, "Diffusion of Na_2O in Sodium in the Range 900 to 1000°F," Report GEAP-3357, General Electric Atomic Power Equipment Dept., San Jose, California, December 21, 1959.
4. L. E. Pohl, "Sodium Mass Transfer: X. 1963 Corrosion Sample Data," GEAP-4437, General Electric Company, San Jose, California, 1964, p. 3.

5. V. J. Rutkauskas, "Determination of the Solubility of Oxygen in Sodium Using the Vacuum Distillation Analytical Technique," Report LA-3879, Los Alamos Scientific Laboratory, in preparation.

6. B. Minushkin and M. Kolodney, "Development of a Continuous Electrochemical Meter for Oxygen in Sodium," Report UNC-5131, United Nuclear Corporation, December 1967, pp. 51 and 84.

7. O. E. Dwyer, High-Temperature Liquid Metal Technology Review, Review No. 663, Vol. 5, No. 5, October 1967, BNL 50089, p. 194.

8. C. C. McPheeters, "Quarterly Status Report on the Advanced Plutonium Fuels Program," April 1 - June 30, 1967, Report LA-3745-MS, Los Alamos Scientific Laboratory, p. 16.

9. V. I. Subbotin, P. L. Kirilov, and F. A. Kozlov, "The Purification of Sodium from Oxygen and Monitoring of Oxygen Content in Sodium," USSR Report 701, 1965.

10. V. I. Subbotin, F. A. Kozlov, E. K. Juznetzov, and N. N. Ivanovskii, "Determination of Oxygen and Hydrogen in Sodium," Alkali Metal Coolants, International Atomic Energy Agency, Vienna, 1967, p. 461.

11. J. P. Delisle, "Automatic Measurement of the Plugging Temperatures of Sodium and Nak," European Atomic Energy Society Colloquium on Liquid Metals, Aix-en-Provence, 1963.

12. D. F. Davidson and P. F. Roach, "An Experimental Continuous-Indication Plugging Meter for Impurity Monitoring in Liquid Alkali Metals," Report TRG-1230, United Kingdom Atomic Energy Authority, Risley, 1966.

13. F. J. Norton, "Gas Permeation through the Vacuum Envelope," in 1961 Transactions of the Eighty Vacuum Symposium and Second International Congress, Vol. I, p. 8, Luther E. Preuss, Editor, New York: Pergamon Press, 1962.

14. H. Ehrhardt and O. Osberghans, Z. Naturforschg. 13a, 16-21 (1958).

15. D. P. Stevenson, J. Chem. Phys. 17, 101 (1949).

16. C. E. Berry, J. Chem. Phys. 17, 1164 (1949).

PROJECT 807

CERAMIC PLUTONIUM FUEL MATERIALS

Person in Charge: R. D. Baker

Principal Investigator: J. A. Leary

I. INTRODUCTION

The principal goals of this project are to prepare pure, well characterized plutonium fuel materials, and to determine their high temperature properties. Properties of interest are (1) thermal stability, (2) thermal expansion, (3) thermal conductivity, (4) phase relationships by differential thermal analysis, (5) structure and phase relationships by x-ray diffraction, high temperature x-ray diffraction, neutron diffraction and high-temperature neutron diffraction, (6) density, (7) hardness and its temperature dependence and (8) compatibility including electron microprobe analysis.

In addition to phase equilibria and general properties, specific thermodynamic properties such as free energy of formation by vaporization equilibria in the 1000-2000°C temperature range with mass spectrometer identification of vapor species, free energy of formation by electromotive force measurement in the 450-1200°C temperature range, and heat capacity and heat of transition are being determined.

II. SYNTHESIS AND FABRICATION

(M. W. Shupe, R. L. Nance, W. M. Jones)

1. Carbides and Nitrides

Approximately 1 cm diam pellets of single phase PuN were prepared for use in electromotive force and vapor pressure measurements. The pellets were pressed and sintered to 92 percent of theoretical density in Ar.

Carbide pellets of $U_{0.8}Pu_{0.2}C_{1.5+x}$ were synthesized for electromotive force measurements. Pellets of $PuC_{0.847}$, $PuC_{0.992}$, $PuC_{1.228}$, and $PuC_{1.343}$ were prepared for use in the mass spectrometer vapor pressure studies. Pellets of $PuC_{0.86}$ were also prepared for differential thermal analysis. In addition to preparation made for properties measurements approximately 20 g of $U_{0.8}Pu_{0.2}C$ carbide powder was synthesized for development of analytical chemistry procedures.

2. Hydrogen Reduction of $(U, Pu)_2C_3/(U, Pu)C_2$ to (U, Pu)C

Conditions for eliminating the presence of higher carbides from $U_{0.8}Pu_{0.2}C$ microstructures have now been defined. The carbide powder containing a slight excess of carbon is reduced to -325 or -230 mesh seive size, then treated with flowing H_2 gas at 850°C. With an exposed powder planar area of 49 cm^2, a treatment time of 0.6 h/g powder produces a powder that can be formed into pure monocarbide pellets. Chemical analysis of powders and pellets are shown in the synthesis and fabrication section of Project 808.

Stainless steel valves to contain (U, Pu)C samples for transport and attachment to oxygen vacuum fusion analysis apparatus were designed and put into operation. Table 807-I gives the oxygen content of material at successive stages in the preparation of pellets for the single set of such measurements for which the valves have been used. Although there still is a considerable scatter

Table 807-I

Oxygen Content of $U_{0.8}Pu_{0.2}C$[1]

(in g O per 10^6 g metal)

Raw Ingot	Annealed Ingot	Powder	Pellet 1	Pellet 2
15, 10, 15	5, 155, 5	170, 250, 210	180, 210, 45	100, 180
15, 15, 10	10, 10, 10	190, 220, 180[2]		

Notes:
(1) Each analysis is a cut from a single sample
(2) This cut analyzed after standing 24 h in sampling valve

to the data, the monocarbide pellets probably contain less than 200 ppm oxygen.

III. PROPERTIES

1. Differential Thermal Analysis

(J. G. Reavis)

Additional DTA observations have been made of the Pu-C system, particularly of the melting of single phase monocarbide. Development of DTA techniques for the determination of heats of fusion is also continuing:

Melting of PuC: DTA observations of two lots of PuC ($PuC_{0.86}$ and $PuC_{0.87}$) have consistently shown thermal arrests at 1605 ± 10°C accompanied by progressive liquid formation at higher temperatures. Easily detectable amounts of liquid were present at 1625° but the pellets did not slump completely until the range 1650-1660° was reached. These temperatures are to be compared with the literature value[1] of 1654° reported as the melting point of PuC, and are consistent with the hypothesis of decomposition of $PuC_{0.86}$ to produce a liquid phase and solid Pu_2C_3 which dissolves in the liquid at higher temperatures, the solubility at 1660° being sufficiently great to give the material the appearance of complete liquefaction.

Heat of Fusion of UO_2-PuO_2: Samples of ZrO_2, UO_2 and UO_2-20% PuO_2 have been cycled through their respective melting points as many as 8 times with no significant mechanical deformation or chemical attack of the sealed W containers. However, W concentrations in the residues were in the range 0.5-1.0%.

To evaluate the change in calculated heats of fusion produced by variation of the amount of oxide sealed in the capsules, a second capsule of ZrO_2 containing 22% less oxide than the first was prepared. The size of the thermal arrest produced by the second sample was 35% less than that produced by the first, thus introducing an uncertainty of about 17% in heats of fusion determined by use of ZrO_2 as a reference material. This uncertainty will be avoided in the future by use of capsules filled with the same number of gram formula weights of reference material as are contained in the capsules of UO_2-20% PuO_2.

Even though the relative magnitudes of the thermal arrests were changed by changing amounts of ZrO_2 in the capsules, the observed melting point did not change (2700 ± 20°C). The observed melting point of UO_2 in a sealed capsule was 2850 ± 20°C.

2. X-Ray Powder Diffraction

(C. W. Bjorklund, R. M. Douglass, J. L. Green)

Additional data have been obtained in the study of self-irradiation damage in plutonium compounds as a function of time, temperature and dose. The lattices of PuO_2, PuN and Pu_2C_3 of normal isotopic composition continue to expand, but at a slower rate, after 1680 d, 1533 d, and 977 d, respectively. The present values of the lattice dimensions are within 92, 98 and 69%, respectively, of the saturation values prediced by the equation

$$a_t = P_1\left(1-e^{P_2 t}\right) + a_o \qquad (1)$$

where a_t is the measured lattice dimension at time t, and P_1, P_2 and a_o are parameters evaluated by a least squares computer technique. a_o is the calculated value of the lattice dimension at time 0, and P_1 is the total expansion at saturation. It was noted in the preceding quarterly report that the lattice of the plutonium compounds enriched with ^{238}Pu have all expanded to saturation values. No further increases have been observed. It was also noted that faint reflections had been detected on films of enriched $PuC_{0.86}$ in positions corresponding to those of Pu_2C_3. These reflections continue to be observed with no detectable increase in intensity. The slow decrease observed for the measured value of the PuC lattice dimension is also continuing.

The lattice expansions of samples of enriched PuO_2 stored at -198°, 25°, 100°, 200° and 400°C have also been measured as a function of time. An empirical equation relating radiation damage (measured by change in lattice dimension) to time which included a temperature

annealing term and which was applicable to PuO_2 over the temperature range 25 to 400°C was reported during the preceding quarter. This equation

$$a_t = (A_1/T + A_2)\left[1-e^{(A_3/T + A_4)t}\right] + a_o \qquad (2)$$

was obtained from Eq. 1 when it was found that although P_1 and P_2 were probably exponential functions of 1/T, plots of P_1 and P_2 were essentially linear over the range 100 to 400°C and deviated only slightly from linearity at 25°C. Accordingly, the equations

$$P_1 = A_1/T + A_2 \qquad (3)$$

and

$$P_2 = A_3/T + A_4 \qquad (4)$$

were substituted in Eq. 1 to give Eq. 2. A more rational expression has now been derived to extend the temperature range to include the data obtained for PuO_2 stored at -198°C, which it was impossible to fit with Eq. 2, as well as to provide a more accurate fit to date obtained over the rest of the temperature range.

$$a_t = \frac{B_1 B_2 a_o}{B_2 + B_3 e^{-B_4/T}}\left[1-e^{-\left(B_2 + B_3 e^{-B_4/T}\right)t}\right] + a_o \qquad (5)$$

This equation is related to Eq. 1 which, in turn, can be derived from the differential equation

$$-\frac{dN}{dt} = \frac{dN^*}{dt} = B_2 N \qquad (6)$$

where B_2 is a rate constant, N is the number of undamaged atoms at time t and temperature T, and N^* is the corresponding number of atoms damaged by self-irradiation of the sample. Integration at constant temperature provides an expression for the fraction N^*/N_o of "damaged" atoms at time t. The assumption that the fractional change in the lattice dimension is proportional to N^*/N_o then leads to Eq. 1. Correspondingly, if an annealing term

$$-\frac{dN^*}{dt} = C(T)N^* \qquad (7)$$

is introduced into Eq. 6, then

$$\frac{dN^*}{dt} = B_2 N - C(T)N^* = B_2(N_o - N^*) - C(T)N^* \qquad (8)$$

where C(T) may be any appropriate function of T. Eq. 5 was derived by integration of Eq. 8 and again assuming that the fractional change in lattice dimension $\Delta a/a_o$ was proportional to N^*/N_o. Because most descriptions of annealing are generally formulated using equations similar to those of chemical kinetics, the function C(T) was taken as

$$C(T) = B_3 e^{-\frac{\Delta E}{kT}}$$

where ΔE represents an average annealing activation energy, and k is the Boltzman constant. In Eq. 5 $\Delta E/k$ was defined as B_4. B_1 is a proportionality constant relating $\Delta a/a_o$ to N^*/N_o, and a_o is the lattice dimension at time 0. The particular form of Eq. 5 which treats a_t rather than $\Delta a/a$ as the independent variable was chosen to avoid the necessity of punching new data decks for the least squares computer program.

A new subroutine was written for the HAP computer program, and the parameters B_1 through B_4 and a_o were successfully evaluated using the combined data for PuO_2 stored at -198°, 25°, 100°, 200° and 400°C. Very good agreement was obtained between experimental data and the curves calculated at each temperature by means of Eq. 5. The values of the parameters and their estimated standard deviations (in parentheses) were:

$B_1 = 3.678 \times 10^{-3}$	(0.5×10^{-3})
$B_2 = 1.136 \times 10^{-2}$	(0.3×10^{-2})
$B_3 = 4.468 \times 10^{-2}$	$(6. \times 10^{-2})$
$B_4 = 1.474 \times 10^{3}$	(0.9×10^{3})
$a_o = 5.3930$	(0.001)

The value of a_o was approximately 0.002 Å lower than

expected, causing the greatest deviation between calculated and experimental results to occur over the 0-18 d interval, where the slopes of the curves were steepest. ΔE was calculated from B_4 ($= \frac{\Delta E}{k}$) to be approximately 0.1 electron volt, which seems to be consistent with the meager data available in the literature. Although these results now tend to justify the validity of the data obtained for PuO_2 stored at -198°C, the question as to whether some annealing still occurs during the interval required to warm the samples to room temperature for x-ray exposure still remains to be resolved.

3. High Temperature X-Ray Diffraction
(J. L. Green)

Development work is continuing on the high temperature furnace for the x-ray diffractometer. Mechanically the system appears to be acceptable. However, studies using NbC samples indicate that relatively small but observable amounts of oxidation occur at 1800°C. Lattice parameter changes as a function of the time at temperature indicate that two separate phases in stoichiometry change occur. During the initial period of the heating cycles (1/2 - 1 h), a relatively large decrease in the apparent C/Nb ratio occurs. This is interpreted as being due to the elimination of oxygen and nitrogen sorbed by the sample prior to heating in the furnace, i.e., the preparation and loading of the sample. An inert atmosphere enclosure is presently being assembled which will allow preparation and loading operations to be carried out without exposing the samples to air. The second phase is a small, continuous decrease in the apparent C/Nb ratio as a function of time. This is felt to be due to continuous sources of oxygen or water vapor in the furnace system. Work is presently being done to eliminate the continuous sources.

4. Thermodynamic Properties of Plutonium Compounds by Electromotive Force Techniques
(G. M. Campbell)

Nitrides: The galvanostatic technique mentioned in the previous report was used to extend the temperature range of the Pu vs PuN emf measurements so that the data now ranges between 714 and 1032°K. After correcting the data to 1 atm N_2 pressure and subtracting the

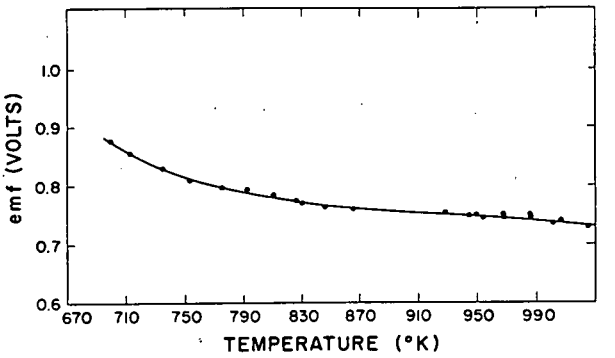

Fig. 807-1 Plot of EMF vs Temperature for the Cell $Pu(s,\ell)/Pu^{+3}$, KCl-LiCl/PuN(s), $N_2(g)$

Ta vs W thermal emf the galvanic emf for the cell

$$Pu(s,\ell)/Pu^{+3},\ KCl\text{-}LiCl/N_2(g),\ PuN(s)$$

is given as

$$E = 7.62768 - 2.22111 \times 10^{-2} T + 2.404858 \times 10^{-5} T^2 - 8.7277 \times 10^{-9} T^3\ (\pm 0.003)\ \text{volts} \qquad (1)$$

where T is in °K. The data are plotted in Fig. 807-1.

The results of previous experiments by an indirect method[2] gave 0.8745 (± 0.005) volts for the emf at 700°K. From the present experiments the emf at this temperature is 0.8701 (± 0.003) volts, which is in good agreement.

The Pu phase change involving the most energy in this temperature range is that of solid to liquid at 913°K. Since this involves only about 1 eu, no change in the slope of the T vs emf plot is detectable. In the region of ϵ-Pu (749-913°K), a least squares analysis of the data gives

$$E = 1.1532 - 4.605 \times 10^{-4} T\ (\pm 0.0016)\ \text{volts}. \qquad (2)$$

Above the melting point of Pu (913°K) the least squares line from the two cells is, as shown in Fig. 807-2:

$$E = 1.0480 - 3.147 \times 10^{-4} T\ (\pm 0.0025)\ \text{volts}. \qquad (3)$$

The decrease in emf with increasing temperature below the melting point of Pu is larger than can be accounted for by consideration of the known thermodynamic properties of the constituents. It seems likely that in the lower temperature range the emf includes a component

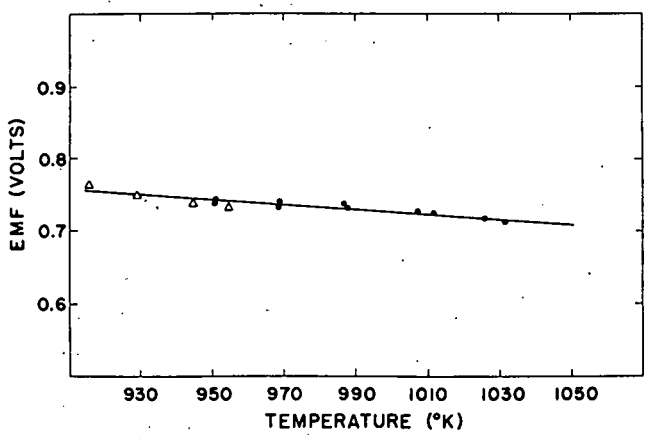

Fig. 807-2 Plot of EMF vs Temperature for the Cell $Pu(\ell)/Pu^{+3}$, LiCl-KCl/PuN(s), $N_2(g)$

Δ = Data points from Cell No. 1
• = Data points from Cell No. 2

that is not related to the free energy change in the Pu-N_2 reaction. Using the data above the melting point of Pu

$$-\Delta G^{o}_{T} = 72.5 - 0.0218\ T \text{ kcal/mole} \qquad (4)$$

for the reaction

$$Pu(\ell) + 1/2\ N_2(g) \rightarrow PuN(s) \quad . \qquad (5)$$

By combustion calorimetry Lapage[3] found $-\Delta H = 70.2 \pm 1.5$ kcal/mole at 298°K for reaction (5). Using the UN data of Godfrey,[4] the U data of Hultgren,[4] the Pu data of Rand[6] and the relation $Cp(PuN) = Cp(UN) - Cp(U) + Cp(Pu)$, it can be shown that $(H_{1000} - H_{298})$ PuN = 8.5887 kcal/mole and $(S_{1000} - S_{298})$ PuN = 14.57 eu. This gives $-\Delta H_{1000} = 72.35$, which is in excellent agreement with the intercept of Eq. (4). Eq. (4) then leads to $-\Delta G^{o}_{298} = 70.3 - 0.0179\ T$ kcal/mole and S^{o}_{298} (PuN) = 18.2 eu. This compares with S^{o}_{298}(UN) = 14.97 eu. If the condition that $S^{o}_{298}(PuN) - S^{o}_{298}(Pu) = S^{o}_{298}(UN) - S^{o}_{298}(U)$ is used, S^{o}_{298}(PuN) = 16.17 eu and from the emf data $-\Delta H^{o}_{298} = 71.9$ kcal/mole. A separate report has been written concerning this system.

Carbides: Three cells of the type

$Pu(\ell)/Pu^{+3}$, LiCl-KCl/$(U_{0.8}Pu_{0.2})_2C_3$ + excess C

were monitored during the period. The galvanostatic technique was used to supplement the liquid Pu electrode so that any transfer of U to the Pu electrode could be detected. None of these cells reached a satisfactory equilibrium, however, A cell of the type

$PuRu_2$ + Ru/Pu^{+3}, LiCl-KCl/$(U_{0.8}Pu_{0.2})_2C_3$ + excess C

is currently being monitored and seems to be giving satisfactory results. The galvanostatic technique of potential determination is being used to supplement the $PuRu_2$ + Ru electrode as a reference. It should be possible to determine in the next few weeks whether this solid solution system can be studied successfully by these electrochemical techniques.

5. Thermodynamic Properties from Vaporization Studies (R. A. Kent)

The mass spectrometric investigation of the system Pu-N has been completed. Over the temperature range 1658-1976°K solid PuN vaporizes according to the reaction

$$PuN(s) = Pu(g) + 0.5\ N_2(g) \qquad (1)$$

with the partial pressure of Pu(g) given by the equation

$$\log_{10} P(atm) = (6.436 \pm 0.055) \frac{-21,953 \pm 98}{T^{o}K} \quad . \qquad (2)$$

The heat of the decomposition reaction is $\Delta H^{o}_{298} = 156.1 \pm 2.5$ kcal. $mole^{-1}$, from which one calculates the standard heat of formation of PuN(s) to be $\Delta H^{o}_{f298} = -73.1 \pm 2.6$ kcal. $mole^{-1}$.

The results of the PuN study together with those of previous studies of the vaporization of plutonium and gold will be presented in LASL Report LA-3902, which is in press.

6. High Temperature Calorimetry (A. E. Ogard, G. Melton)

The high temperature heat contents and heat capacities of $U_{0.8}Pu_{0.2}O_{2.00}$ and $U_{0.8}Pu_{0.2}O_{1.98}$ are being determined as part of a cooperative program with GE-Sunnyvale. In addition, these properties are being determined for UO_2 and α-Al_2O_3. To date the measurements have been completed up to ~2400°K in a drop calorimeter that was not enclosed in a glovebox. At these high temperatures, grain growth is extensive in the welds of the W capsules used to contain the oxides. Therefore the calorimeter has been relocated in a plutonium handling enclosure, and the calorimeter is being recalibrated.

An additional high temperature furnace with a W mesh heating element has been fabricated for use with the calorimeter. This furnace has been operated up to 2800°K in vacuum.

IV. ANALYTICAL CHEMISTRY

1. Determination of Uranium and Plutonium in Mixed Carbides and Oxides (G. B. Nelson, K. S. Bergstresser, and G. R. Waterbury)

A new transistorized controlled-potential coulometer developed at LRL was applied to the determination of U and Pu. When solutions of the pure metals were used as sample material, the method showed no bias for either element, but when (U, Pu)C ingots were used as sample material the method was unbiased with respect to Pu but results for U were approximately 0.2 percent higher than those obtained by potentiometric titration. This investigation is being continued. Relative standard deviations of the method were 0.03 and 0.1 percent respectively for the Pu and U.

2. Determination of Oxygen in $(U, Pu)O_2$ (C. S. MacDougall, M. E. Smith, and D. E. Vance)

Three methods are being investigated in which O_2 is liberated as CO and CO_2 by inert-gas-fusion at 2,000°C from an oxide fuel-C pellet and then measured either gravimetrically, gas chromatographically, or by microwave discharge spectrometry.

Various parameters in the gas chromatographic finish were investigated to obtain optimum operating conditions. Good peak separations were obtained with a 12-ft column of activated charcoal, but all grades of charcoal tried introduced organic contaminants which made this column unsatisfactory. A 24-ft silica gel column is now being tested with Xe as the internal standard.

Previous measurement of the CO and CO_2 by microwave discharge spectrometry showed that the relative standard deviation of this method was 1.3 percent. Conditions to stabilize the gas flow through the spectrometer cell, integration of the peak areas using a new electronic integrator, and the use of homogeneous U_3O_8 samples are being investigated in an attempt to improve the precision.

Repeated analyses of a high-purity ThO_2 and U_3O_8, using an automatic temperature programmer, showed that the inert-gas-fusion method was not biased and the relative standard deviation was 0.1 percent. The apparatus was installed in a glovebox suitable for analyses of $(U, Pu)O_2$ materials and the work will be continued.

3. Determination of O/M Ratios in $(U, Pu)O_2$ (J. W. Dahlby and G. R. Waterbury)

A gravimetric method reported by Lyon (GEAP Rpt. 4271, 1963) produced high O/M ratios (between 2.006 and 2.008) for UO_2 when this material was oxidized in air in the recommended manner and then reduced in $He-H_2$ as the sample was heated from room temperature to 950°C. Experiments performed using a thermobalance showed that introduction of the reducing gas mixture while the sample was at 950°C produced $UO_{2.001}$ with a standard deviation of 0.001. Under these same conditions, mixtures containing 4 grams of U and 1 gram of Pu produced oxides having low O/M ratios, 1.991 to 1.998. The reasons for these low results are being investigated by determining conditions that produce stoichiometric PuO_2 from Pu metal.

4. Electron Microprobe Examinations of (U, Pu)C, Pu_2C_3 and U, Pu)O_2 (E. A. Hakkila and H. L. Barker)

Approximately thirty samples of (U, Pu)C from various experiments were examined to identify precipitates, inclusions, and phases, and to determine homogeneity. In most specimens the matrices were homogeneous with respect ot U, Pu, and C distributions on a macroscale although a few were heterogeneous on a microscale. Precipitates and inclusions generally were enriched in Pu, depleted in U and C, and contained Si and often Fe. Some also contained W, a few contained Cu, and one was Pu alone. White phases were enriched in U and depleted in Pu, and low density phases were enriched in Pu, depleted in U and C, and contained Cu, Fe, Ni, and Si. A white phase in a Pu_2C_3 specimen contained less C than the matrix. The diffusion zone of a UC-PuC diffusion couple was found to be approximately 200-μ wide. The C content in this zone was low as compared to either carbide. Grain boundary diffusion of Pu into the UC was observed. White particles in a

$(U, Pu)O_2$ matrix were identified as W containing some Fe but no U, Pu, Ta, or Si.

5. Miscellaneous Analytical Services (N. L. Koski, G. B. Nelson, M. E. Smith, L. E. Thorn, and W. W. Wilson)

Approximately forty samples of (U, Pu)C materials from various preparatory operations and experiments were analyzed for U, Pu, C, N, and/or H by controlled-potential coulometric, combustion, and Kjeldahl methods. Uranium concentrations ranged between 72.8 and 76.3 percent, Pu between 18.3 and 19.85 percent, C between 3.98 and 7.58 percent, N generally between 65 and 840 ppm with a few samples containing between 0.37 and 0.49 percent, and H between 10 and 70 ppm. For eighty-three measurements of oxygen in these materials by an inert gas fusion method, most of the values were between 5 ppm and 0.1%, but three were near the 1 percent level. Four (U, Pu)C samples were prepared for mass spectrometric measurement of isotopic compositions. In ten PuN samples analyzed, the Pu concentrations ranged between 90.1 and 93.8 percent, N between 4.8 and 5.4 percent, and O_2 between 150 ppm and 0.13%. The Pu concentrations found in three PuC samples were in the range from 94.5 to 94.9 percent, C ranged between 4.18 and 4.24 percent, O_2 between 240 ppm and 0.19 percent, and N was 130 ppm.

V. REFERENCES

1. R. Mulford, et al. in Plutonium 1960, (Grison, Lord and Fowler, eds), 1961, p. 301, Cleaver Hume Press, London.
2. G. M. Campbell and J. A. Leary, J. Phys. Chem. 70, 2703 (1966).
3. R. Lapage and J. L. Bunce, Trans. Faraday Soc. 63, 1889 (1967).
4. T. G. Godfrey, J. A. Woolley, and J. M. Leitnaker, "Thermodynamic Functions of Nuclear Materials: UC, UC_2, UO_2, ThO_2, and UN", ORNL-TM-1596 (1966).
5. R. Hultgren, R. L. Orr, P. D. Anderson and K. K. Kelley, "Selected Values of Thermodynamic Properties of Metals and Alloys", John Wiley & Sons Inc., New York (1963).
6. M. H. Rand, IAEA 4, Special Issue No. 1 Plutonium, Vienna (1966).

PROJECT 808

COMPATIBILITY OF SODIUM-BONDED (U,Pu)C AND (U,Pu)N FUELS WITH CLADDING MATERIALS

Person in Charge: D. B. Hall
Principal Investigators: R. H. Perkins
J. A. Leary

I. INTRODUCTION

The use of sodium for heat transfer between the fuel pellets and the cladding is desirable to lower the surface temperature of the pellets and to permit substantial tolerances in the dimensions of the pellets and the clads. The objectives of this program are to study and understand the interactions of (U,Pu)C and (U,Pu)N with sodium and potential cladding materials and, if necessary, to modify the properties of these components to achieve a satisfactory sodium-bonded fuel element for a LMFBR. Emphasis is to be placed on the studies of sodium-bonded carbides in Type 316 stainless steel.

The assembly of equipment and the development of procedures is continuing. In addition, however, literature surveys were completed on the compatibility of (U,Pu)C fuel[1] and (U,Pu)N fuel,[2] respectively. The data on the carbide fuel invariably emphasize the difficulty in obtaining single-phase, stoichiometric monocarbide, and several reports document the unsuitability of the hypostoichiometric form or that containing dicarbide. The nitride fuel is comparatively easy to prepare in a pure form that is compatible with stainless steel. Considerable remains to be done with both fuels with respect to compatibility in- and out-of-pile, and regarding the techniques of preparation, handling, metallography, and analysis.

The effect of different post-test procedures for removing bond sodium on the pore distribution and size was studied as the initial step in pre- and postirradiation examination of carbide fuels.[3] The structure of sintered (U,Pu)C was studied by metallography after removing the sodium bond by dissolution and distillation. The porosity after sodium removal was compared to unbonded "as-received" pellets. The data show that a low temperature distillation technique is the preferred method for removing sodium from sodium bonded fuel capsules.

Carburization of stainless steel clad through sodium has received some attention in this laboratory[4] and warrants further study relative to the compatibility of (U,Pu)C. In addition to integral tests of compatibility in- and out-of-pile, more specialized studies of the following nature should also be pursued:

1. The effects of venting fuel capsules to the sodium coolant.
2. The effects of high concentrations of fission products in sodium bonds on compatibility.
3. The stability of the sodium bond under various stresses.

II. CARBIDE FUEL COMPATIBILITY STUDIES
(F. B. Litton, L. A. Geoffrion, J. H. Bender)

A. General

The objectives of this program are to study the interactions among single-phase mixed uranium-plutonium carbide, a sodium bond, and potential cladding materials, i.e., to investigate the technology related to sodium-bonded fuel elements. There are two approaches to the experimental work. One approach is to determine the reactions occurring between $(U_{0.8}Pu_{0.2})C$ and potential cladding materials, using Type 316 stainless steel and a high-strength vanadium-base alloy (V-15Ti-7.5Cr) as the first and

second choices of cladding material, respectively. A second concurrent set of experiments is to study the mechanism of carbon transport through sodium, the effect of impurities such as oxygen, and the carburizing potential of sodium in mutual contact with carbides and the preferred cladding materials.

Capsules containing sodium-bonded, single-phase (U,Pu)C will be tested in sodium loops at 750°C for periods up to 10,000 h. Primary emphasis will be placed on fundamental reactions occurring between $(U_{0.8}Pu_{0.2})C$ and Type 316 stainless steel or vanadium alloy. High-purity, thoroughly characterized sodium will be used for the studies. Fuels of known composition will be supplied using methods developed by the Ceramic Plutonium Fuel Materials (807) program at LASL. Most of the testing will be performed on stoichiometric (U,Pu)C fuel; hypo- and hyperstoichiometric mixed carbides will also be studied to determine the effect of the M/C ratio of the fuel on carbon transport by the sodium bond. Carbides containing known and controlled amounts of oxygen and nitrogen will be tested to determine the effect of these additives on the sodium bond and on fuel-clad compatibility. The Pu/U ratio in most mixed fuels will be maintained at 0.2, but some experiments will be performed on stoichiometric and hyperstoichiometric UC to determine the effect of plutonium addition on the behavior of the carbide fuel.

B. Current Results

1. Mechanism of Carbon Transfer

Apparatus for studying the mechanism of carbon transfer in the carbide-sodium-container system was assembled and tested prior to loading with 300 g sodium. The apparatus is shown on page 28, Report LA-3880-MS. Provision was made in the apparatus to getter the sodium with zirconium and to add carbon to the system by introducing a carbon-containing gas into the purified helium cover gas.

2. Compatibility of Clad with Sodium-Bonded Carbide Fuel

The test capsules for these compatibility studies were loaded in the Fuel Loading Facility. Each Type 316 stainless steel capsule (0.30-in. o.d. by 0.10-in. wall by 3-in. long) was loaded with three (U,Pu)C fuel pellets (0.265-in. diam by 0.25-in. long) and one length (0.24-in. diam by 1-in. long) of extruded sodium rod. After the closure welds were made, the capsules were removed from the drybox, heated to 600°C (1112°F) for 1 h and centrifuged while cooling to room temperature. They were reheated to 300°C (572°F) and placed in a magnetostrictive device for 1 h. The integrity of the bond was verified by inspection using x-ray, ultrasonic, and eddy-current techniques.

Three capsules were tested in a forced-convection sodium loop operating at 750°C for 1000 h. After the test, the capsules were inverted at temperature in an effort to separate the bonding sodium from the fuel. Residual sodium was removed from the pellets by vacuum distillation at 500°C.

Analyses of the loop sodium during test and the bond sodium after test are shown in Table I.

Table I

Analyses of Sodium Used in 750°C Compatibility Test

Element	Concentration, ppm: Convection Loop	Concentration, ppm: Bond Sodium
Li, Be, Ag	< 1	< 1
Ba	< 10	< 1
Mg, V, Mn	< 1	1
Cr, Co, Ni, Sr, Mo	< 3	< 3
Al, Si, Pb, Bi, Ti	< 3	< 5
B	< 3	< 8
Cu	8	8
Cd	< 30	< 10
Fe, Sn	< 10	15
Ca	< 1	20
K	15	*
Zn	<300	<300
C	--	42
Pu	--	0.8
U	--	6

*Not reported.

The concentrations of uranium, plutonium, and carbon in the bond sodium indicate either solubility of these elements or particulate suspension during test. Further tests will be run at lower temperatures and with larger quantities of bonding sodium to verify these results.

Examination of the Type 316 stainless steel cladding by metallographic, electron microprobe, and microhardness techniques indicated that no reaction had occurred between clad and fuel. A sample

of the cladding was prepared for ^{3}He activation analysis, but this was not completed during this reporting period.

The fuel pellets were primarily single-phase (U,Pu)C (Fig. 1) containing very minor quantities

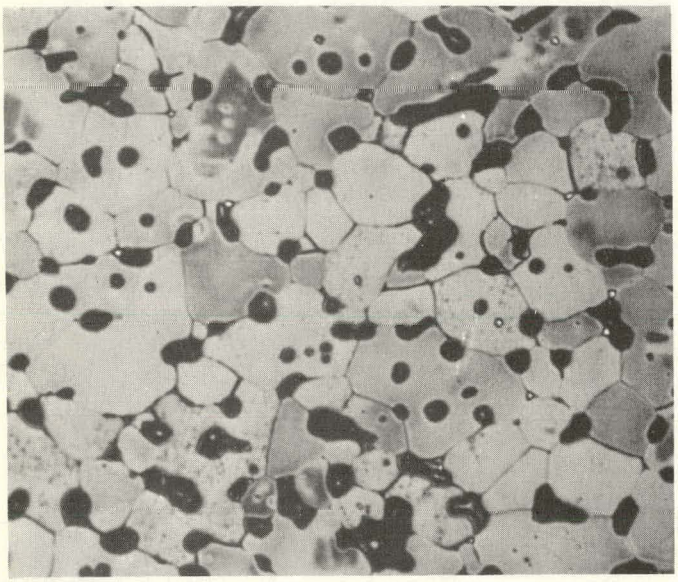

Fig. 1. Typical structure of essentially single-phase mixed carbide fuel pellets. Electro-etched, 300X.

of spheriodal metal phase. The porosity was 10.6%. A widening of the grain boundaries at the sodium contact surfaces was noted. This is shown in Fig. 2. Associated with the boundary widening was

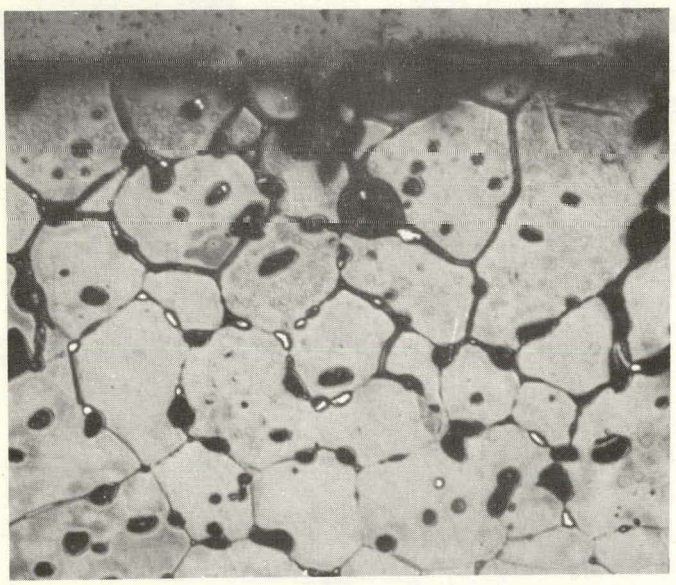

Fig. 2. Typical structure at the sodium contact surface. Electro-etched, 300X.

a greater quantity of the metal phase. The structure of the Type 316 stainless steel clad material is shown in Figs. 3 and 4. There was no evidence

Fig. 3. Structure of Type 316 stainless steel capsule indicating no carburization during test period. Etched, 300X.

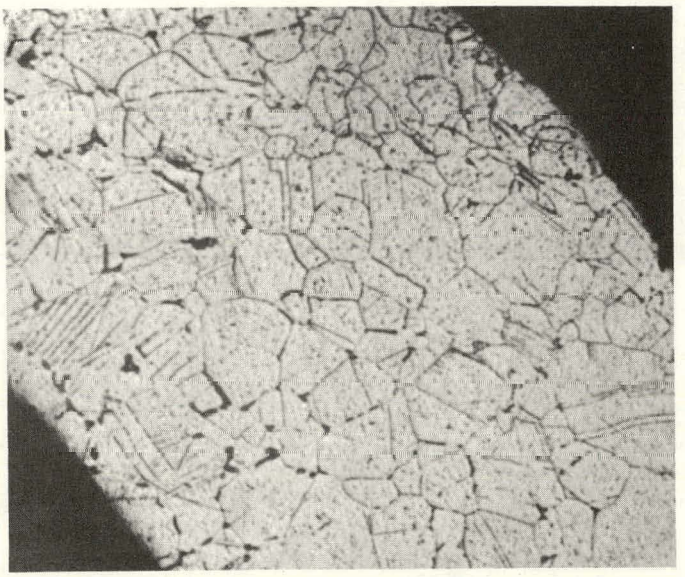

Fig. 4. Capsule closure cap showing no structural change during test period. Etched, 300X.

of any change in structure, such as carburization, during the test period.

Microhardness measurements were made on transverse sections of the clad material. Indentions were made as near as practical to the contact surface and in the center of the tubing. Average

values were 191 DPH at the inside surface and 198 DPH (100 g load) near the center.

The intensities of the carbon, chromium, iron, nickel, and molybdenum x-rays were measured at 5 to 25 micron intervals from the inner to the outer surface of the capsule. No significant variation in intensities as a function of location were observed for any of the elements. The relative standard deviations for measuring chromium, iron, nickel and molybdenum intensities were 2.4, 0.9, 1.1, and 13 per cent, respectively.

3. Corrosion Study

The behavior of selected cladding materials in zirconium-gettered sodium is being investigated as a function of temperature. Groups of six specimens each of V, V-10Ti, V-20Ti, V-40Ti, V-15Ti-7.5Cr, Type 304L and 316L stainless steel, Nb-1Zr, and Nb-10W were immersed in a forced-convection sodium loop at 650°C for 1000 h. (Specimen analyses and reports of earlier tests are given in LA-3820-MS and LA-3880-MS.)

The weight changes recorded in Table II indicate no significant corrosion of these materials in low-oxygen sodium at 650°C. Films were detected on the vanadium alloys, but the amounts were insufficient for x-ray diffraction analyses. Further tests are in process for longer periods at 750°, 650°, and 550°C.

Table II

Corrosion of Materials in Hot-Trapped Sodium at 650°C for 1000 h

Material	Heat Treatment	Weight Change* (mg/cm^2)
V	Annealed 1 h, 900°C	- 0.023
V-10Ti	Annealed 1 h, 900°C	+ 0.029
V-20Ti	Annealed 1 h, 900°C	+ 0.044
V-40Ti	Annealed 1 h, 900°C	+ 0.108
V-15Ti-7.5Cr	Annealed 1 h, 850°C	+ 0.241
Type 304L SS	Annealed 1 h, 1000°C	- 0.037
Type 316L SS	Annealed 1 h, 1000°C	- 0.040
Nb-1Zr	Annealed 1 h, 1350°C	+ 0.021
Nb-10W	Annealed 1 h, 1350°C	- 0.006

*Average of six one-half inch square specimens.

Specimens which had been tested in hot-trapped sodium were subjected to electron microprobe examination. The objective of the examination was to determine whether a deplection of elements occurred near the surface of the specimen. The samples that were examined are listed below:

Type 304 stainless steel tested at 650°C for 1000 h.

Type 304 stainless steel tested at 750°C for 1000 h.

Type 316 stainless steel tested at 650°C for 1000 h.

V-20Ti tested at 650°C for 1000 h.

V-20Ti tested at 750°C for 1000 h.

V-15Ti-7.5Cr tested at 650°C for 1000 h.

V-15Ti-7.5Cr tested at 750°C for 1000 h.

The results of these examinations are as follows:

Type 304L and 316L Stainless Steel

Intensities of iron, nickel, chromium, silicon, and carbon x-rays were measured at 10-micron intervals across each of the samples, and also at randomly selected areas near the edges and near the centers of the samples. Significant differences in intensities of x-rays for these elements were not observed between the edges and interiors of the samples. Sodium was not detected; the detection limit for sodium in stainless steel is estimated to be in the range between 0.1 and 1 per cent.

V-20Ti

Intensities of titanium and vanadium x-rays were measured at 10-micron intervals across each of the samples, and also at randomly selected areas near the edges and near the centers of the samples. For the 650°C specimen some enrichment of vanadium and depletion of titanium was detected to a depth of approximately 20 to 30 microns from the sample edge. However, for the specimen heated at the higher temperature, significant differences in titanium and vanadium x-ray intensities were not detected between the edge and the interior of the sample.

V-15Ti-7.5Cr

Intensities of titanium, vanadium, and chromium x-rays were measured at 10-micron intervals across each of the samples, and at randomly selected areas near the edges and centers of the samples. Significant differences in intensities of the x-rays for these elements were not observed between the edges and interiors of the samples.

III. VENTED (U,Pu)C EXPERIMENTS
(J. C. Clifford)

A. General

Sodium and single-phase (U,Pu)C are being contacted in a small forced-convection sodium system for periods of 1000 h and longer. The experiments are limited to determining the out-of-pile stability of single-phase (U,Pu)C in flowing sodium in support of studies of fission product release from the same material during and after neutron irradiation.

B. Current Results

After a 2200-h exposure to 700°C sodium, three capsules were examined. Two of the capsules had apertures at the top and bottom, allowing sodium to flow through the capsule. The third capsule was closed at the bottom to maintain an environment of static sodium around the pellets. Midway during the testing period the loop developed a serious sodium leak and was shut down. The capsules were transferred under helium to an inert-gas storage can, the damaged loop section was replaced, and the loop was recharged. Cartridges of zirconium foil, inserted one after another over a 1400-h period, were used to remove oxygen from the system. At the end of this cleanup period the vented capsules were returned to the loop and the test was completed without further incident. No oxygen analyses were conducted on loop sodium prior to the failure, so that the length of time during which the oxygen concentration was above normal, and the oxygen levels attained, are unknown. However, it is certain that significant amounts of oxygen were introduced into the system; the hot trap contained extensive precipitates of zirconium oxide. As a result of the leak, the behavior of the fuel and clad are thought to be atypical, but nevertheless of interest.

After sodium had been removed from the capsules by vacuum distillation, metallographic and microprobe examinations were conducted on fuel and clad. The fuel pellets showed no unusual features except for localized precipitation of an acicular phase along the surfaces and edges of pellets from all capsules (Fig. 5). A slight increase in pellet porosity was noted (< 4% change), but this may have resulted from incomplete removal of sodium from the fuel during the distillation step.

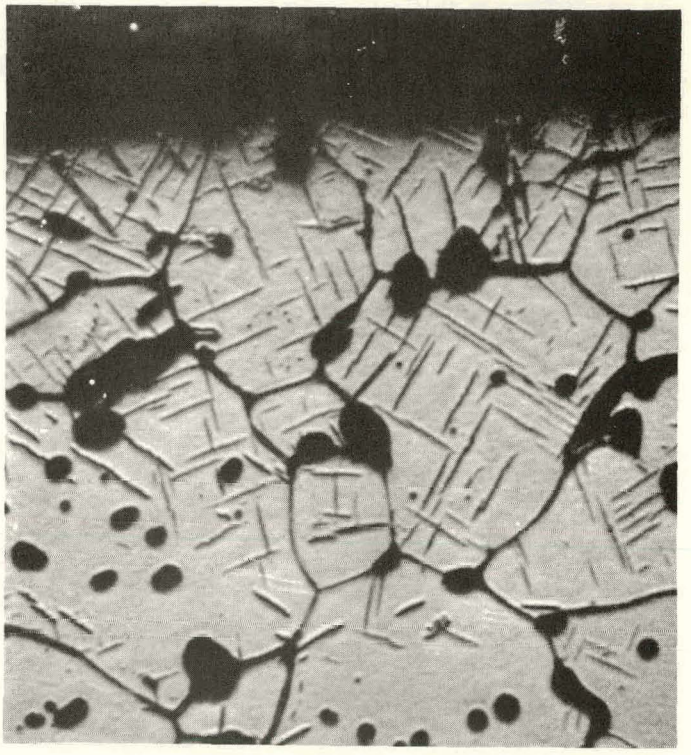

Fig. 5. Surface of a (U,Pu)C fuel pellet after a 2200-h exposure to 700°C sodium. An acicular phase has developed. Electro-etch followed by chemical etch, 400X.

Some changes were found in the 10-mil, Type 316 stainless steel clad of all three capsules; the static bond capsule was less affected than the two flow-through capsules. The outside surfaces of all capsules exhibited a thin film (∿ 0.2 mil, max) depleted in iron, chromium, and manganese and enriched in nickel with respect to the matrix. No evidence of intergranular attack was seen. The inner surface of the static bond capsule exhibited no significant peculiarities; however, both flow-through capsules contained carbide precipitates in regions adjacent to the fuel pellets (Figs. 6 and 7). Precipitation was not continuous over the entire fueled zone of either capsule; at intervals along the carburized surfaces, precipitate-free zones were visible (the light areas visible at the metal surface in Fig. 7). The composition of these zones has not been established.

Because of the peculiar behavior noted in these capsules, another 2000-h test is being conducted in hot-trapped, 700°C sodium. The capsules will be available for examination after April 6.

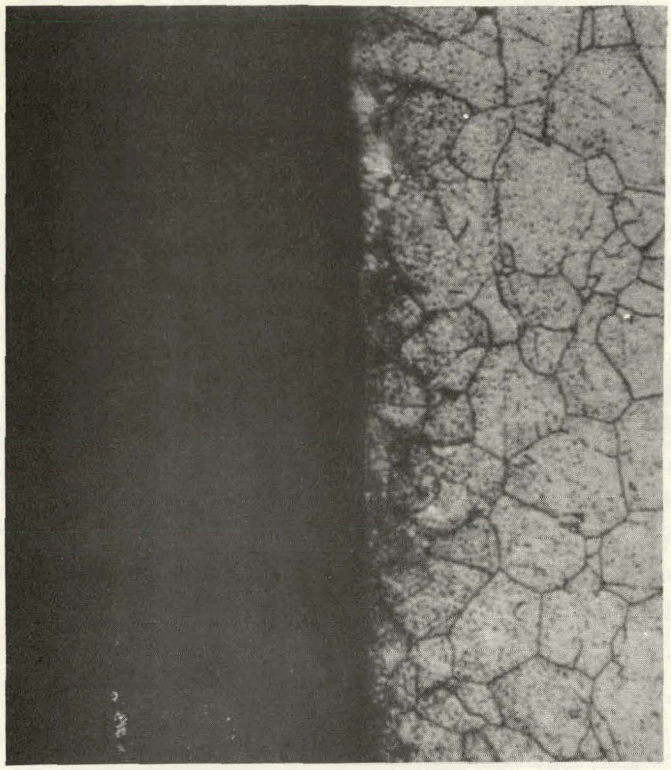

Fig. 6. Inside surface of a flow-through, Type 316 stainless steel capsule after 2200 h in 700°C sodium. Some carburization has occurred. Electroetch, 600X.

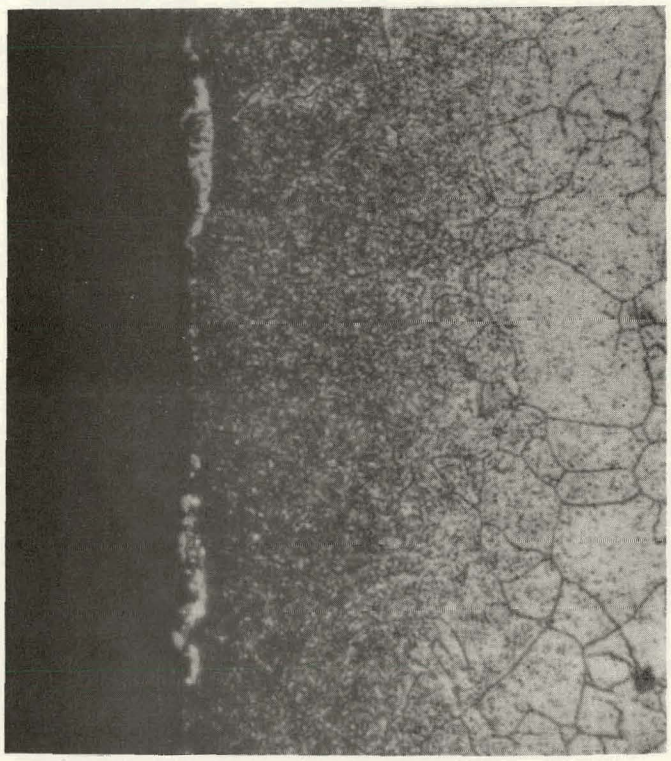

Fig. 7. Same capsule as Fig. 6. Carbide precipitates and a reaction layer are visible. Electroetch, 600X.

IV. LOADING FACILITY FOR TEST CAPSULES (D. N. Dunning)

A. General

The sodium and (U,Pu)C fuel capsule loading facility is operational, although not complete. The primary function of the facility is to produce test capsules loaded with sodium and fuel pellets and free from contaminants other than any initially present in the fuel. An inert atmosphere box for the handling and inspection of (U,Pu)C fuel pellets is being assembled.

B. Current Results

1. Fuel Loading Station

A new two-section, evacuable, inert atmosphere glovebox is being assembled and equipped for use in loading the fuel pellets into capsules. Transfer of the pellets into the test capsules will be made through the bulkhead of the box from the "alpha hot" to the "alpha cold" section. A semi-automatic pellet measuring device and micro surface examination equipment are being installed in this box.

The present fuel loadings are carried out in the sodium loading box using aluminum foil lining to control contamination.

2. Sodium Purification Loop, Sodium Loading Box, and Sodium Bonding

This equipment continues to be operational on a routine basis.

3. EBR-II Irradiation Capsule Loading

Two EBR-II irradiation capsules were loaded during this reporting period. Fifty-three (U,Pu)C fuel pellets plus four UC pellets were loaded into each capsule using the loading procedure illustrated in Fig. 8. The capsules were then bonded using the standard procedure. Nondestructive tests showed that the first capsule contained a number of chipped and cracked fuel pellets. This capsule was rejected for the initial irradiation in EBR-II. No defects were detected in the second test capsule, so it was loaded into a secondary container. After sodium bonding and final nondestructive examination, this capsule was sent to EBR-II. Analytical samples were taken of the sodium used in all loadings.

V. POST-TEST EXAMINATION
(J. H. Bender)

A. General

Metallographic examination is one of the primary methods for evaluating the compatibility of fuels with cladding; however, delineation of the phases that may be present in sintered (U,Pu)C (metallic, dicarbide, and sesquicarbide) has been inaccurate with all of the known metallographic techniques. Continued investigation of multiple techniques has succeeded in developing a stain etch, microhardness, microhardness and preferential etch method that accurately distinguishes between the metallic, dicarbide, and sesquicarbide phases of (U,Pu)C and precipitates of PuSi.

B. Current Results

Additional electron microprobe analyses of the phases and precipitates in sintered (U,Pu)C samples have proven the reliability of the stain-etch, microhardness test, and preferential etch as a quick method for distinguishing between the metallic, dicarbide, and sesquicarbide phases of (U,Pu)C and precipitates of PuSi.

A glovebox for inert atmosphere metallographic preparation has been received and is being prepared for operation. The inert box will be utilized for (U,Pu)C sectioning and diamond grinding. In addition, it may be used for the metallographic preparation of sodium samples using a technique that is now under investigation.

VI. EBR-II IRRADIATION TESTING
(J. O. Barner)

A. General

The purpose of these irradiations is to evaluate candidate fuel/sodium/clad systems for the LMFBR program. In the reference design, pellets of single-phase (U,Pu)C are separated by a sodium bond from a cladding of Type 316 stainless steel or other high-temperature alloy. Seven fuel-element tests are planned in the initial group of a continuing series of EBR-II irradiation experiments.

The capsules are to be irradiated under the following conditions:

1. Lineal power: 29.15 to 30.20 kW/ft (max).
2. Fuel composition: $(U_{0.8}Pu_{0.2})C$, (single-phase, sintered, fully enriched).
3. Fuel density: 85% and 90% of theoretical.
4. Smear density: 75% and 80%.
5. Clad size: 0.300 in. o.d. x 0.010 in. wall.
6. Fuel size: 0.265 in. diam x 0.25 in. high.
7. Clad type: 316 SS and Hastelloy-X.
8. Maximum clad temperature: 1250°F.
9. Maximum fuel centerline temperature: 2130°F.
10. Burnup: 0.22 to 0.66 g fissioned per cm^3.

B. Current Results

Procedures for loading the EBR-II capsules were selected after loading tests with a mockup capsule. After completion of nondestructive testing on the mockup, the first of the planned irradiation capsules (designated LASL-42) was loaded and bonded. During nondestructive testing, chips of fuel were found in the sodium bond. These chips were sufficient grounds for rejection of the capsule for the initial set of irradiation experiments in EBR-II.

A second capsule (designated LASL-42B) was loaded, bonded, and nondestructively tested. No chips were found in the capsule and eddy-current tests indicated satisfactory bonds, and all welds appeared to be sound. The capsule was shipped to EBR-II for insertion in the X011 subassembly. Final nondestructive testing at EBR-II revealed a small tungsten deposit in a weld of the outer containment. The nondestructive test procedures used at EBR-II and LASL are essentially identical; however, inspection of all parts of the weld for minute defects is very difficult, and it was apparently only by chance that the small tungsten acclusion was detected in the second, but not the first, of the radiographic tests. The LASL-42B capsule will be returned to LASL for repair of the reject weld. It should be available for insertion in EBR-II about April 15, 1968.

The remainder of the initial seven-pin complement will be available for insertion during the first quarter of fiscal 1969.

VII. THERMAL FLUX IRRADIATIONS
(J. O. Barner, R. L. Cubitt, D. C. Kirkpatrick)

A. General

The Omega West Reactor (OWR) has been used for preliminary testing of fueled capsules which are mockups of those intended for fast flux irradiations in EBR-II.

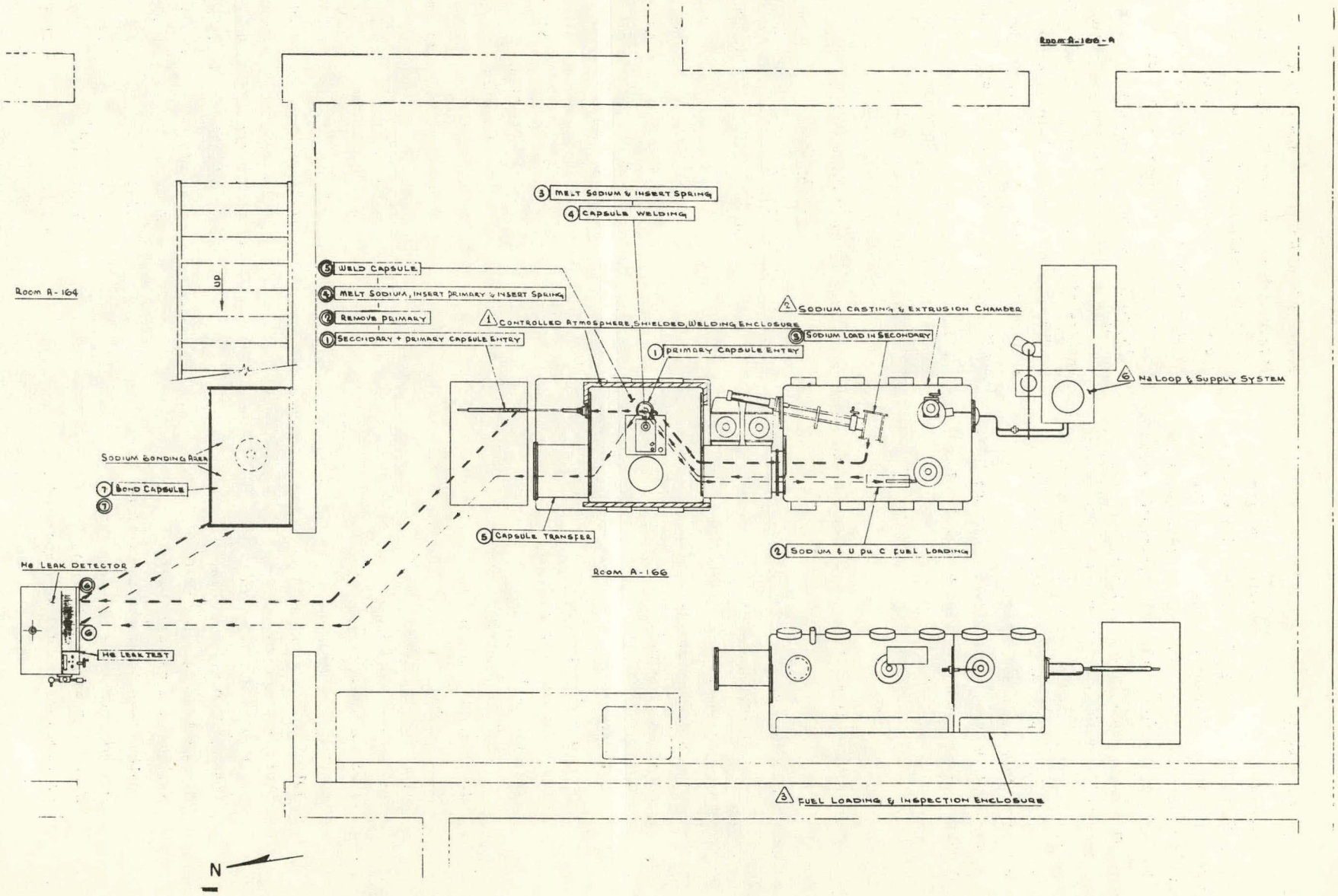

Fig. 8. Fuel loading facility.

B. Current Results

A mockup of the EBR-II capsules was irradiated in the Omega West Reactor for 113 h. The experiment was designated OWREX-10; the test capsule held three pellets of $(U_{0.8}Pu_{0.2})C$ which contained 1.58 g Pu and 5.79 g ^{235}U. Table III illustrates a comparison between OWREX-10 and LASL-42B. OWREX-10 was operated at 1.19 times the maximum heating rate expected in EBR-II, and at a 50°F higher maximum mean inner pin temperature. The maximum burnup at the fuel surface was ∿ 5900 MWD/T.

OWREX-10 has been destructively analyzed in the hot cells. All welds and hold-down devices had operated satisfactorily. The pellets were recovered intact with no apparent cracks or chipping. They were later inadvertently exposed to air while being cleaned with butyl alcohol and they disintegrated. No carburization of the Type 316 stainless steel or of the Type 316 stainless steel pellets immediately adjacent to the fuel was observed. A small amount of ^{133}Xe was found in the pin gas plenum and small amounts of ^{131}I, ^{140}La, and ^{137}Cs were found in the bonding sodium. The OWREX-10 experiment indicated that there are no serious errors in the design or construction procedures of the EBR-II capsules.

Table III

Physical, Dimensional and Operating Characteristics of OWREX-10 and LASL-42B

	OWREX-10	LASL-42B
Lower blanket	316 SS	^{238}UC
Fuel (U enrichment 93%)	$(U_{0.8}Pu_{0.2})C$	$(U_{0.8}Pu_{0.2})C$
Upper blanket	316 SS	^{238}UC
Fuel hold-down spring	Nb	Nb
Bonds and reservoir	Na	Na
Inner pin	316 SS	316 SS
Outer pin	304 SS	304 SS
Pin centering device	316 SS	316 SS
Pin hold-down spring	308 SS	308 SS
All weld design	Identical	
All hold-down design	Identical	
Lower blanket length, in.	0.750	1.000
Fuel length, in.	0.750	13.250
Upper blanket length, in.	0.250	0.250
Sodium reservoir length, in.	2.50	5.25
Fuel hold-down spring, inc.	9.25	22.01
Inner pin length, in.	10.973	36.637
Total capsule length, in.	12.313	39.80
Fuel diameter, in.	0.265	0.265
Inner pin o.d., i.d., in.	0.300 x 0.280	0.300 x 0.280
Outer pin, o.d., i.d., in.	0.375 x 0.335	0.375 x 0.335
Average heating rate, kW/ft	39.5	25.85
Maximum heating rate, kW/ft	35.9	30.20
Maximum mean outer pin temperature, °F	1038	1067
Maximum mean inner pin temperature, °F	1250	1200
Maximum inner pin heat flux, Btu/h-ft^2	1.53×10^6	1.26×10^6
Maximum fuel centerline temperature, °F	∿ 1950	∿ 2130

VIII. GAMMA SCANNING AND OTHER STUDIES

(D. M. Holm, J. L. Parker, W. M. Sanders, B. M. Moore, H. M. Ruess)

A. General

Work on improved gamma-scanning techniques continues, and equipment to measure short-lived fission-product yields from fast-neutron-induced fission in plutonium has been constructed. The ^{3}He activation technique for the determination of oxygen and carbon in germanium and carburized stainless steel is also being investigated.

B. Current Results

1. Gamma Scanning of EBR-II Fuel Pins*

Three EBR-II driver fuel pins were gamma scanned to determine the distribution of fission products and activation products. The Ge(Li) anticoincidence gamma-ray spectrometer was used, and the spectra were unfolded to determine the spatial distributions of the isotopes. The existing scanners and cave were modified to accommodate the extra length of the samples.

From spectra taken at different positions, 22 gamma-ray lines have been analyzed. Table IV shows the energies of the lines, the isotope identification, and the method of production. Figures 9 through 14 show some typical results from an axial scan of one of the fuel pins, LASL #4. The bottom of the fuel is at 2.6 in. and the top at 16.2 in.

Table IV

Gamma-Ray Energies Observed in EBR-II Driver Fuel Pins

Gamma-Ray Energy (keV)	Isotope	Reaction
2186	^{144}Pr	Fission
1490	^{144}Pr	"
1332	^{60}Co	$^{59}Co(n,\gamma)^{60}Co$
1173	^{60}Co	"
1050	^{106}Rh	Fission
834	^{54}Mn	$^{54}Fe(n,p)^{54}Mn$
810	^{58}Co	$^{58}Ni(n,p)^{58}Co$
765	^{95}Nb	Fission
757	^{95}Zr	"
724	^{95}Zr	"
695	^{144}Pr	"
662	^{137}Cs	"
620	^{106}Rh	"
512	^{106}Rh	"
512	^{58}Co	$^{58}Ni(n,p)^{58}Co$
497	^{103}Ru	Fission
144.7	^{141}Ce	"
133.5	^{144}Ce	"
116	Unidentified	Unidentified
112	"	"
100	"	"
97	"	"

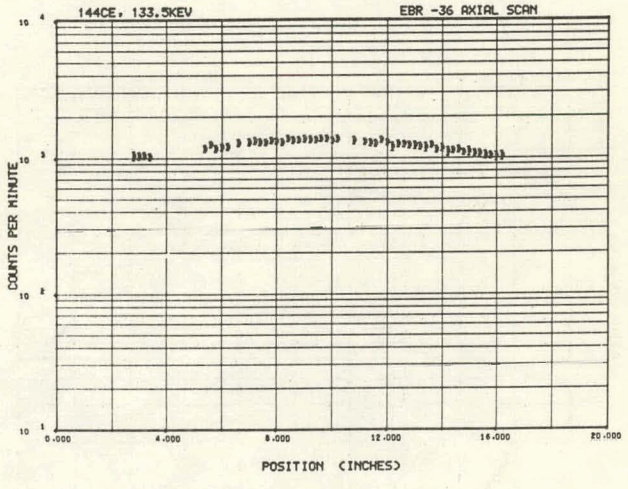

Fig. 9. ^{144}Ce distribution in LASL #4. Typical results from a gamma scan of an EBR-II fuel pin. The bottom of the fuel is at 2.6 in. and the top at 16.2 in. The scan was done with a slit 0.20 in. high, 0.5 in. wide, and 8 in. long.

*See also Project 822, Section IX.

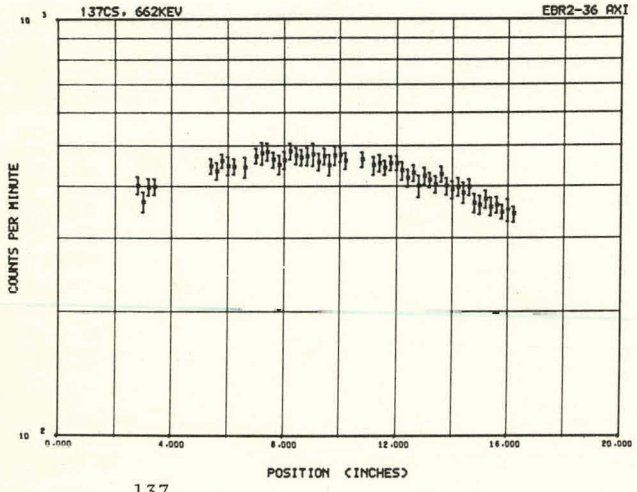

Fig. 10. ^{137}Cs distribution in LASL #4. Typical results from a gamma scan of an EBR-II fuel pin. The bottom of the fuel is at 2.6 in. and the top at 16.2 in. The scan was done with a slit 0.20 in. high, 9.5 in. wide, and 8 in. long.

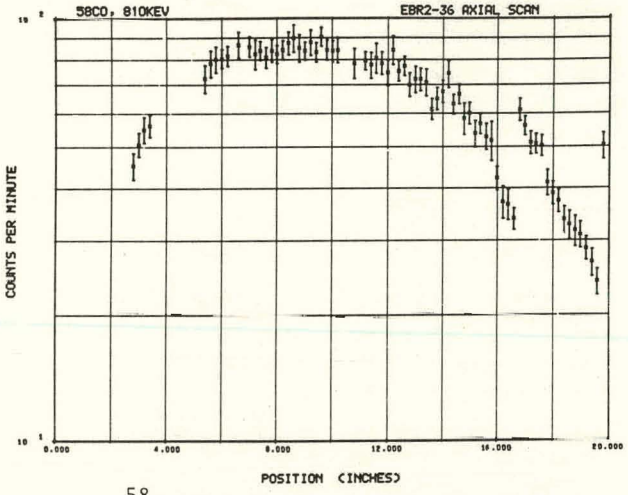

Fig. 12. ^{58}Co distribution in LASL #4. Typical results from a gamma scan of an EBR-II fuel pin. The bottom of the fuel is at 2.6 in. and the top at 16.2 in. The scan was done with a slit 0.20 in. high, 0.5 in. wide, and 8 in. long.

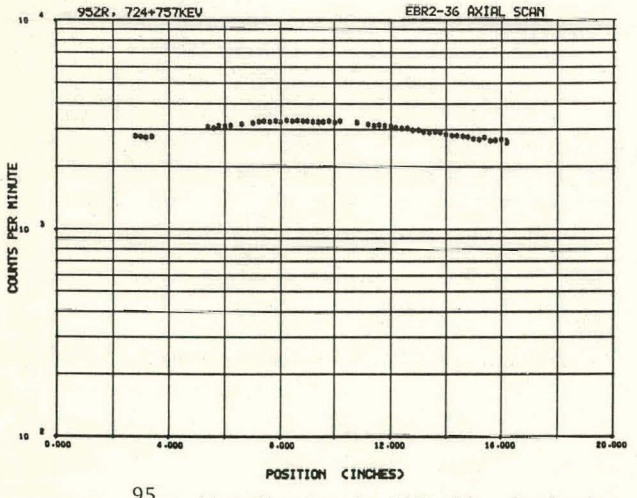

Fig. 11. ^{95}Zr distribution in LASL #4. Typical results from a gamma scan of an EBR-II fuel pin. The bottom of the fuel is at 2.6 in. and the top at 16.2 in. The scan was done with a slit 0.20 in. high, 0.5 in. wide, and 8 in. long.

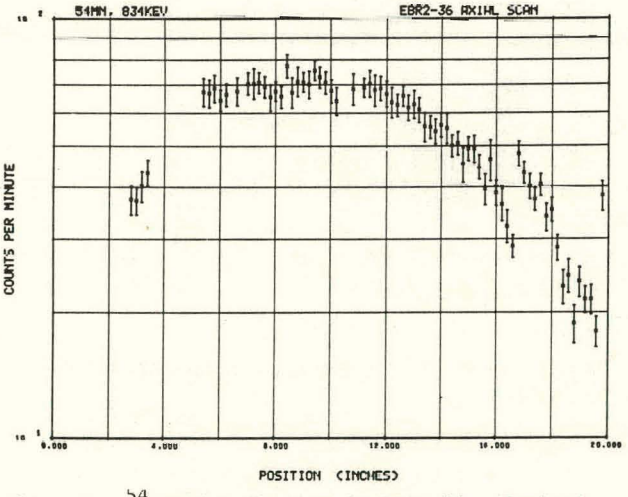

Fig. 13. ^{54}Mn distribution in LASL #4. Typical results form a gamma scan of an EBR-II fuel pin. The bottom of the fuel is at 2.6 in. and the top at 16.2 in. The scan was done with a slit 0.20 in. high, 0.5 in. wide, and 8 in. long.

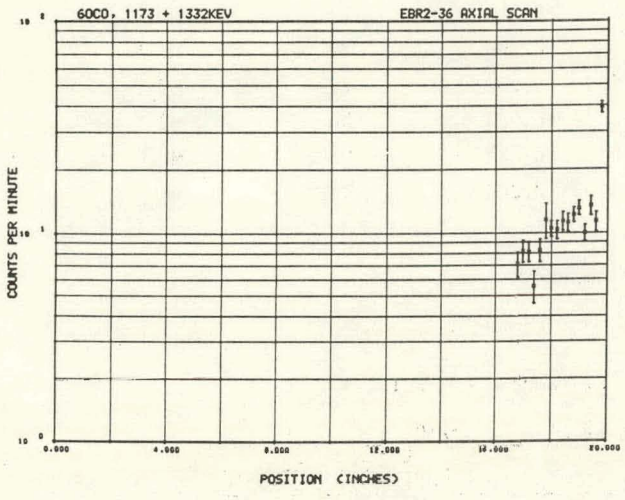

Fig. 14. ^{60}Co distribution in LASL #4. Typical results from a gamma scan of an EBR-II fuel pin. The bottom of the fuel is at 2.6 in. and the top at 16.2 in. The scan was done with a slit 0.20 in. high, 0.5 in. wide, and 8 in. long.

The scan was done with a slit 0.20 in. high, 0.5 in. wide, and 8 in. long. Spectra were taken every 0.2 in. with 40 min of counting. Some of the spectra were not analyzed because of trouble with the tape transport. All fission products had similar distributions, and no evidence of migration has been observed. Axial buckling is evident; the fission rate in the center of the pin is about 30% greater than at the top and bottom.

The most interesting observations to date are with regard to the effects of neutron energy on the distributions. As noted above, the fission rate in the center plane is about 30% higher than at the ends of the fuel (Figs. 9-11). However, in the center plane of Figs. 12 and 13, the fast neutron activation products of stainless steel increase to nearly 3 times the values at the ends. The sharp discontinuity at the top fuel surface is from a stainless steel retaining rod inside the capsule. The distribution of ^{60}Co, a thermal activation product (Fig. 14), is opposite that of the fast neutron activation products shown in Figs. 12 and 13. No ^{60}Co was detected in the fueled region of the capsule.

Diametrical scans of the capsules with an 0.031-in.-diam pinhole are being analyzed, and no segregation of fission products has been observed.

2. Gamma Scanning of Short-Lived Fission Products from Fast Fission of Plutonium

The automatic sample changer described in the last report of this series has been connected to the Nuclear Data 4096-channel analyzer. The systems function together as designed, but there is a slight problem of electronic noise. Work has begun on the Hydro critical assembly to make it acceptable as a fast fission neutron source for these experiments.

3. ^{3}He Activation

Germanium. Several samples of germanium were irradiated to assess the problem of oxygen surface contamination. It appears that surface contamination has been a problem in the past, and our techniques for eliminating it were not adequate. During the next 3-5 months, no new irradiations will be possible because the accelerators are being connected in series for three-stage operation.

Carburized Stainless Steel. Standard samples of normal and low carbon stainless steel, as well as samples of graphite, tantalum oxide, and a metal potting compound have been irradiated; autoradiographs were made during the measurement of the activation product decay curves.

The results at this time indicate that the potting compound has an induced activity comparable to that in the stainless steel, the spatial resolution is about 0.001 in., and NTB-2 track plates have a sensitivity about 10 times that of NTB plates in this application. The measurement of the absolute calibration of the system is not complete.

IX. SYNTHESIS AND FABRICATION

(M. W. Shupe, C. A. Emery, H. G. Moore, R. W. Walker, A. E. Ogard)

A. General

Procedures have been developed for synthesizing and producing (U,Pu)C and (U,Pu)N pellets for compatibility testing. The recent effort has been directed toward producing fully enriched $(U_{0.8}Pu_{0.2})C$ pellets for EBR-II irradiation experiments which require 52 pellets per pin. The present available inventory for this experiment is 382 pellets. No effort has been allocated for preparation of nitride pellets for compatibility testing.

Table V

Characteristics of Fully Enriched $U_xPu_yC_z$ Pellets

Lot No.	X	Y	Z	Quantity	Diameter (in.)	Density (% theor.)	Microstructure[1]
6-71-1	0.792	0.208	0.988	16	0.265	...	MC,I
6-82-2	0.796	0.204	0.990	58	0.266	...	MC,I
6-86-1	0.802	0.198	...	50	0.266	89	MC,I
6-88-1	0.802	0.198	...	46	0.266	89	MC,I
6-106-1	0.796	0.204	0.977	80	0.264	90	MC
6-115-1	0.800	0.200	...	69	0.265	91	MC
6-126-1	0.796	0.204	...	59	0.265	92	MC

Note (1): MC = monocarbide only.

MC,I = monocarbide plus < 0.5 v/o metallic impurity.

Table VI

Typical Spectrochemical Analysis of Powders and Pellets

	Concentration of Element, $g/10^6$ g Pu			
	Lot 6-86-1		Lot 6-88-1	
Element	Powder	Pellet	Powder	Pellet
Li	< 1	< 1	< 1	< 1
Be	< 1	< 1	< 1	< 1
B	< 1	< 1	< 1	< 1
Na	5	< 2	2	< 2
Mg	5	< 5	< 5	< 5
Al	20	< 10	< 10	< 10
Si	65	65	60	< 20
P	< 50	< 50	< 50	< 50
Ca	< 5	< 5	< 5	< 5
Ti	< 50	< 50	< 50	< 50
V	< 5	< 5	< 5	< 5
Cr	< 10	< 10	< 10	< 10
Mn	< 2	5	< 2	< 2
Fe	30	55	30	< 20
Co	< 5	< 5	< 5	< 5
Ni	< 10	15	< 10	< 10
Cu	20	50	20	25
Zn	< 10	< 10	< 10	< 10
Sr	< 5	< 5	< 5	< 5
Nb	< 50	< 50	< 50	< 50
Mo	< 10	< 10	< 10	< 10
Cd	< 10	< 10	< 10	< 10
Sn	5	< 2	< 2	< 2
Ba	< 10	< 10	< 10	< 10
W	15	40	< 10	15
Pb	...	< 2	< 2	...
Bi	< 2	< 2	< 2	< 2

Carbide pellets are produced by the following method:

1. Multiple arc melting of U, Pu, and C on a 60 g scale using a graphite electrode.
2. Solution treatment of the ingot.
3. Crushing and grinding in a WC vibratory mill, followed by screening the resulting powder.
4. Reduction of excess carbon by reaction with folowing H_2.
5. Cold compaction followed by sintering in flowing argon.

B. Current Results

During this period 76 pellets were delivered for use in compatibility studies, and 119 pellets of (U,Pu)C plus 10 pellets of UC were delivered for EBR-II irradiations.

Characterization of the 7 lots of pellets produced during this period is summarized in Table V. At this time evaluation is not fully complete. Experience to date indicates that a H_2 treatment time of 0.4 h/g will eliminate MC_2 and M_2C_3 from the pellet microstructures in most cases. Pellets produced after lot No. 6-82-2 were treated at a rate of 0.6 h/g and all the microstructures were free of higher carbide phases. Of the 250 pellets from lots 6-71-1 through 6-106-1, all have been examined radiographically and 16 were rejected because they were found to have internal cracks.

In the previous report it was shown how reduction of impurities could be attained by using purer melting stock. Further reduction to very low impurity levels in pellets has been attained. Typical powder and resulting pellet impurity concentrations are shown in Table VI. Experience has shown that very low impurity levels are necessary before clean pellet microstructures can be attained.

Typical analysis for O, N, and H are on the order of 250, 400, and < 10 ppm, respectively. A typical photomicrograph of pellet microstructure is shown in Fig. 15. A typical lattice dimension is 4.965 ± 0.001 Å.

Particle size distributions of H_2 reduced (U,Pu)C powders are shown in Table VII. The arithmetic mean diameters of the 4 lots show a consistency of particle size when process conditions are controlled.

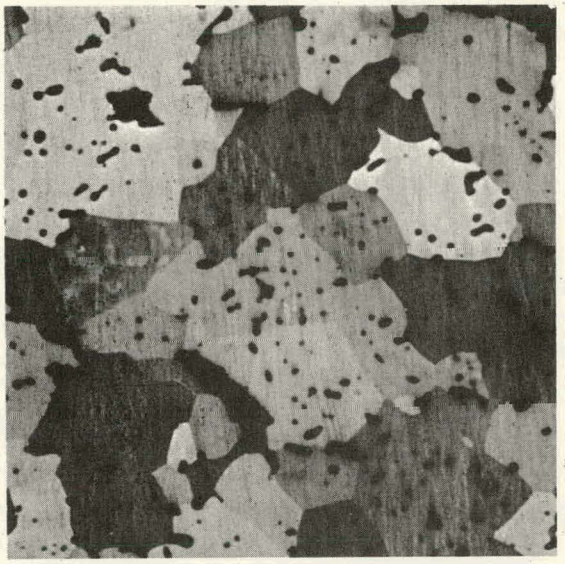

Fig. 15. Typical single phase $(U_{0.8}Pu_{0.2})C$ (Lot 6-115-1). Delta electrolysis etch, 380X.

Table VII

Particle Size Distribution of Hydrogen Treated $U_{0.8}Pu_{0.2}C$ Powders
(By Sedimentation Balance)

Lot No.	Maximum Size Mesh	Maximum Size (μ)	Tap Density	Mass Median Diam
6-74-1	230	64	3.8	19.5
6-81-1	230	64	3.3	21.0
6-86-1	230	64	2.8	18.4
6-88-1	230	64	2.9	15.8

X. ANALYTICAL CHEMISTRY
(A. L. Henicksman, E. A. Hakkila, H. L. Barker, K. S. Bergstresser, O. R. Simi)

A. General

Specific analytical techniques have been developed and evaluated to cope with the problems encountered in the investigation of fuel-clad compatibility and in the general development of sodium technology. While the results of many of these special analyses are given in several sections of the report in Projects 801 and 808, the analytical techniques themselves have not been described. A brief summary of some of the techniques, and the problems to which they were applied, is given below.

B. Current Results

1. The Determination of Uranium and Plutonium in Sodium

Compatibility studies involving sodium bonded (U,Pu)C encapsulated in Type 316 stainless steel have required a method for determining uranium and plutonium in the sodium. Plutonium is determined by alpha-counting but uranium must be determined by a chemical method. The uranium is separated from the sodium by being adsorbed from 8 M HNO_3 as U(IV) on Dowex 1 x 8 resin, eluted with 0.1 M HNO_3. Nitric acid is then removed by evaporation of the solution to dryness with HCl. The uranium is reduced to U(II) with zinc and Arsenazo III is added to form the colored complex whose absorbance is measured at 670 mμ. To date all work has been done on known solutions, but the method will be applied to actual sample materials.

2. Microprobe Examination of Alloys and (U,Pu)C Materials

The following services have been performed on materials involved in compatibility studies:

Approximately 10 (U,Pu)C samples that had been in molten Na for 2000 h were examined to determine homogeneity on a macroscale and to identify precipitates. The U, Pu, and C were homogeneously distributed on a macroscale. The more-common precipitate was enriched in Pu, depleted in U and C, and contained Si. A few precipitates were found that were depleted in U and Pu, and contained significant amounts of Si and Al. Five stainless steel specimens that had contacted (U,Pu)C or molten Na were examined to determine concentration gradients, diffusion of C and Cu, and to identify reaction layers and precipitates. Concentration gradients for Fe, Ni, Cr, Mo, and C were not found in the matrix materials. A slight diffusion of Cu from a surface layer into two specimens was observed. The reaction layers were enriched in Ni and depleted in Fe, Cr, and Mn. Precipitates contained either Mn-Si-Cr, Mn-S-Cr, or Mn-Cr. Of two V-Ti alloys and two V-Ti-Cr alloys that had contacted Na at 650° to 750°C for 1000 h only one V-Ti alloy showed that reaction had occurred. A surface layer, 20 to 30 microns thick, was enriched in V and depleted in Ti in this alloy.

3. Investigation of Distillation Residues from the Vacuum Distillation of Metallic Sodium

Fabrication of the equipment for measuring impurities in sodium was completed, and initial assembly of the components was made in the shops. The equipment was then disassembled for minor modifications and for reassembly as a component part of the inert-atmosphere enclosure system. This reassembly with the inert system will be made without disrupting the atmosphere which presently is at a level of about 1 ppm O_2 and 6 ppm H_2O following 3 weeks of operation. It is anticipated that continued operation of the inert system will gradually reduce the moisture level to 1 ppm. Final assembly of the equipment probably will be completed within 1 month, and vacuum distillations of sodium started.

4. Spectrochemical Analysis of Sodium

An electrode-sample preparation developed at WAPD[5] was modified for our requirements. This involves dissolution of the Na metal in ethanol, conversion to NaCl, evaporation to dryness, mixing with Sp-2 graphite powder and exciting with a dc arc. Table VIII shows the limits of detection for the various impurity elements. It is expected the method will be applicable to hot cell use for the analysis of irradiated samples.

Table VIII

Tentative Limits of Detection for Impurity Elements in Sodium

Element	Limit of Detection (ppm)	Element	Limit of Detection (ppm)
Li	0.8	Cu	3
Be	0.8	Zn	300
B	3	Ga	3
Mg	0.8	Sr	0.8
Al	3	Y	3
Si	3	Mo	3
K	3	Rh	3
Ca	0.8	Ag	0.8
Ti	3	Cd	3
V	0.8	In	3
Cr	3	Sn	3
Mn	0.8	Ba	0.8
Fe	0.8	Au	3
Co	3	Pb	3
Ni	3	Bi	3

5. Miscellaneous Analytical Services

Six samples of sodium metal that had contacted irradiated plutonium fuel materials were analyzed for total sodium and fission-product elements. Two sodium cold traps made of Type 316 stainless steel loaded with graphite rods were analyzed for Pu, Ce, and fission-product elements. Preparation of these samples for analysis required acid leaching of the stainless steel and burning of the graphite followed by dissolution of the ignition residue. Three stainless steel samples that had been in contact with sodium at 750°C for 1000 h were analyzed by a combustion method for carbon; the values obtained ranged from 35 to 50 ppm. Analyses by an inert gas fusion method of four zirconium foils taken from sodium hot traps showed that the O_2 concentrations ranged between 0.30 and 32 per cent as compared to 780 ppm in the original zirconium foil.

REFERENCES

1. F. B. Litton, "The Properties and Irradiation Behavior of Carbide Fuels: A Literature Survey," Report LA-3799, Los Alamos Scientific Laboratory, March 14, 1968.

2. B. J. Thamer, "The Use of (U,Pu)N Fuel with A Sodium Bond: A Summary of Existing Data," Report LA-3646, Los Alamos Scientific Laboratory, March 27, 1967.

3. F. B. Litton and J. H. Bender, "The Removal of the Sodium Bond from (U,Pu)C Fuel Pellets," submitted to Nuclear Applications.

4. F. B. Litton and L. A. Geoffrion, "Quarterly Status Report on the Advanced Plutonium Fuels Program, April 1 - June 30, 1967," Report LA-3745-MS, Los Alamos Scientific Laboratory, August 30, 1967, p. 53.

5. Private communication, John Herb, Westinghouse Electric Corporation, to L. D. Kirkbride, Los Alamos Scientific Laboratory.

PROJECT 811

REACTOR PHYSICS

Person in Charge: D. B. Hall
Principal Investigator: G. H. Best

I. INTRODUCTION

Basic to the evaluation of fast breeder concepts and proposals are the analytical techniques and physical data used in the analyses. Valid comparisons between different concepts and proposals depend on minimization of differences in results due to the methods of analysis. To this end, the Los Alamos Scientific Laboratory is cooperating with other AEC laboratories and contractors in the development of evaluated cross-section data and associated processing codes. This work is coordinated by the Cross Section Evaluation Working Group (CSEWG), which is made up of representatives of the various organizations. In addition, the Laboratory is working on the development and maintenance of digital computer programs pertinent to the nuclear analysis of fast breeder concepts. Finally, the Laboratory is evaluating the performance characteristics of various fast breeder reactor concepts.

II. CROSS-SECTION PROCUREMENT, EVALUATION, AND TESTING (M. E. Battat, D. J. Dudziak, R. J. LaBauve)

A. General

Accurate predictions of reactor design parameters, such as critical mass, sodium worth, and spectral response, require the development and maintenance of up-to-date basic microscopic nuclear data files. To meet this need, a national cooperative program is in progress to prepare an evaluated nuclear data file (ENDF/B).

B. Data Testing

Calculations have been performed for three selected critical experiments, using multigroup constants derived from the Category I ENDF/B library data. The experiments selected for study were:

1. a bare plutonium-metal assembly - JEZEBEL
2. a uranium-reflected ^{235}U metal assembly - TOPSY
3. a dilute plutonium-fueled assembly surrounded by a depleted uranium reflector - ZPR-3 Assembly 48.

For all three systems, critical masses and central reactivity worths were computed; in addition, central activation ratios were calculated for ZPR-3 Assembly 48. Calculations were compared with experiment and with results obtained from the UKAEA and LRL neutron data contained in the LASL library. Results are summarized in Tables I through VI. This work was presented at the Second Conference on Neutron Cross Sections and Technology, held March 4-7, 1968, in Washington, D.C.

TABLE I

CALCULATED AND MEASURED CENTRAL SPECTRA

Percent of Total Flux - ENDF/B Cross Sections

E_{lower}	$\phi_{calculated}$ JEZEBEL	TOPSY	ZPR3/48	$\phi_{experiment}$ ZPR3/48*
6.065 MeV	2.36	1.23	0.42	
3.679	9.04	5.72	1.71	
2.231	16.27	12.29	3.81	
1.353	18.73	16.22	5.47	
0.821	17.73	16.60	7.31	
0.498	14.37	15.77	9.90	10.85
0.302	9.95	13.27	11.94	11.36
0.183	5.69	8.87	12.01	10.85
0.111	3.04	5.14	10.15	10.31
67.4 keV	1.75	2.74	8.88	8.97
40.9		1.31	7.20	7.13
24.8	0.86	0.65	6.77	5.83
15.0		0.13	5.64	4.76
9.12		0.04	3.42	3.85
5.53	0.19		2.08	2.80
3.35			1.40	1.82
2.03			0.42	1.27
1.23			0.85	
748 eV			0.43	
454			0.14	
214			0.05	

*Normalized as follows:
Sum of measured fluxes = sum of corresponding calculated fluxes

TABLE II

CALCULATED AND EXPERIMENTAL CRITICAL MASSES
ENDF/B CROSS SECTIONS

JEZEBEL Pu contains 4.5% ^{240}Pu.
TOPSY U is enriched to 94.1% ^{235}U.

System	Calculated (kg)	Experiment (kg)
JEZEBEL	15.65 Pu	16.28 Pu
TOPSY	15.9 U	17.4 U
ZPR-3/48	339 ^{239}Pu*	272 ^{239}Pu**

*Calculated homogeneous sphere
(R_{core} = 49.78 cm) = 337.1 kg
Homogeneous cylinder = 337.1/0.927 = 363.6
Heterogeneous cylinder = 363.6 - 25.0 = 338.6
k_{eff} = 0.975 for R_{core} = 47.42 cm

**Heterogeneous cylindrical mass.

TABLE III

JEZEBEL - CENTRAL REACTIVITY WORTHS
cents/mole

Material	ENDF/B	UKAEA	LRL	Experiment
Fe	- 27.2	- 22.2		- 21.5
Ni	- 60.1	- 54.6		- 48.0
^{235}U	929.	821.	798.	804.
^{238}U	87.	103.	98.	114.
^{239}Pu	1763.	1557.	1591.	1592.
^{240}Pu	1091.	983.	855.	1038.

TABLE IV

TOPSY - CENTRAL REACTIVITY WORTHS
cents/mole

Material	ENDF/B	UKAEA	LRL	Experiment
^{6}Li	- 70.2	- 72.8		- 130.4
^{7}Li	0.004	3.0		7.9
Be	9.1	8.9		9.2
Fe	- 2.4	- 2.7		- 2.2
Mo	- 6.7		- 5.8	- 3.5
^{235}U	212.7	216.8	207.3	208.4
^{238}U	25.4	21.5	28.7	26.7
^{239}Pu	392.5	396.4	403.4	402.6
^{240}Pu	221.	210.	168.	286 ± 14

C. Shielding

An evaluation of neutron interaction and photon production cross sections for sodium, magnesium, chlorine, potassium, and calcium was recently completed by Drake,[1] and the data were presented in an extension of the United Kingdom (UK) data file format.[2] As part of the LASL effort on the CSEWG, the sodium data were translated to the extended ENDF/B

TABLE V

ZPR-3 ASSEMBLY 48 - CENTRAL REACTIVITY WORTHS
cents/mole

Material	ENDF/B	UKAEA	LRL	Experiment*
C	- 0.21	- 0.04	- 0.21	- 0.017
Na	- 0.19	- 0.07		- 0.046
Cr	- 0.279			- 0.149
Fe	- 0.287	- 0.18		- 0.204
Ni	- 0.443	- 0.32		- 0.325
Mo	- 1.78		- 0.49	- 1.27
^{235}U	26.8	23.3	23.9	24.1
^{238}U	- 2.02	- 1.87	- 1.56	- 1.80
^{239}Pu	35.4	31.9	35.0	32.2
^{240}Pu	6.56	2.94	- 7.0	5.87

*Values were converted from central perturbation cross sections to cents/mole.

TABLE VI

ZPR-3 ASSEMBLY 48
CENTRAL ACTIVATION RATIOS RELATIVE TO ^{235}U FISSION
ENDF/B CROSS SECTIONS

(1.0-cm radius central region)

Type	Calculated	Experiment
^{238}U fission	0.0332	0.0307
^{238}U (n,γ)	0.158	0.138
^{239}Pu fission	0.960	0.976
^{240}Pu fission	0.248	0.243

format (extended to include photon data[3]), and a copy of these data was sent to the National Neutron Cross Section Center (NNCSC) at BNL, where they will use the data as a test set for extending the checking code CHECKER to include the photon production data and data for inelastic scatter to discrete levels. The data will then be plotted by the NNCSC, where possible, for comparison with the sodium evaluation presently on the ENDF/B file. A review of the two sets of sodium data will be performed by LASL. The ENDF/B version of Drake's sodium data is also being sent to ORNL for review. The magnesium, chlorine, potassium, and calcium data will be translated into the extended ENDF/B format when the final version of the data is available in the extended UK format.

The translations were performed by two LASL codes written for this purpose: LUTE, which translates the photon data, and LATEX, which translates neutron data and makes a complete ENDF/B tape. Both codes, along with flow diagrams, are being sent to

ORNL to assist in constructing a general UK↔ENDF/B translation code. Some parts of the UK→ENDF/B translation could not practically be automated, such as the general file 1 data in ENDF/B, which has no counterpart in the UK data file. Also, the photon production data from inelastic scatter were entered in ENDF/B by hand, using the transition probability option which is available only in ENDF/B format.

The translation of Drake's sodium data is the first set of photon production data in the ENDF/B format, which will be useful for debugging the data retrieval codes for photon data. A code is now being written at LASL to extract photon production matrices for use with photon transport codes. The code, called LAPH, will compute pointwise (in energy) photon production cross sections and average them over N arbitrary neutron energy groups, for G arbitrary photon energy groups. The resulting N x G matrix can then be used in conjunction with neutron-group flux vectors to prepare the spatially dependent photon source term for photon transport codes such as QAD, MCG, or DTF-IV. Figure 1 is a schematic diagram of the code.

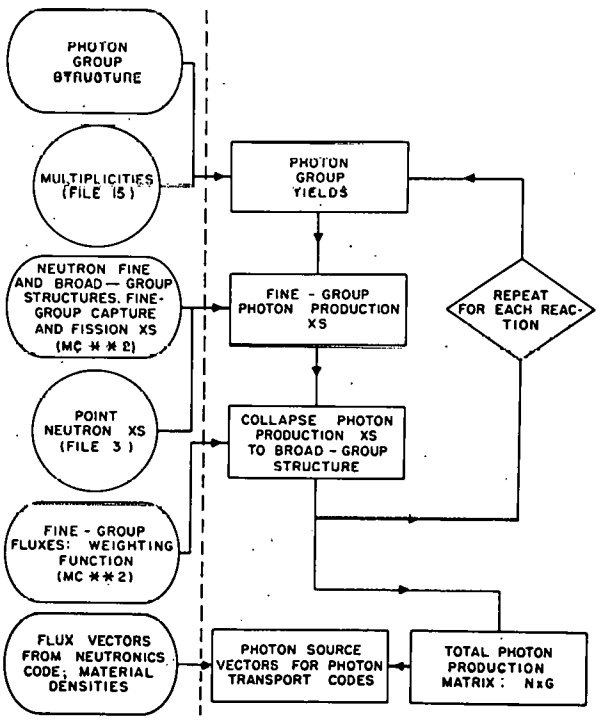

Fig. 1. Schematic diagram of LAPH code. This code extracts photon production matrices from ENDF/B data for use with photon transport codes.

III. REACTOR ANALYSIS METHODS AND CONCEPT EVALUATIONS

A. Space-Time Reactor Kinetics Codes

1. Synthesis Method (J. C. Vigil). The GAKIN code[4] has been compiled on the CDC-6600 computer. GAKIN is a one-dimensional multigroup diffusion theory kinetics code which incorporates the following features:

1. Solutions for slab, cylindrical, or spherical geometry.
2. Arbitrary number of neutron energy groups.
3. Arbitrary number of regions and space points.
4. Optional inclusion of xenon poisoning.
5. Time-dependent cross sections.
6. Optional inclusion of external sources.
7. Arbitrary number of delayed neutron groups.

GAKIN is an extension of the WIGL2 code[5] to the multigroup case, except it does not include thermal feedback. Comparisons will be made between results from GAKIN and results from the code developed at LASL.

2. Multienergy-Group Methods (G. C. Hopkins). Preliminary comparison runs have been made with the monoenergetic transient analysis code ANCON[6] and its multigroup equivalent, ANCONMG. Data representing \$1.50 and \$0.65 reactivity insertions were prepared by ONEDAC for input to ANCON, and by PARAM for input to ANCONMG. The analysis employed UHTREX data, a step reactivity insertion, and two feedback lumps (fuel and moderator). When delayed neutrons were included, the Keepin 6-group parameters[7] were used. Results are shown in Table VII.

Physical or numerical phenomena effecting analytical differences in the results will be analyzed in a later report. A few brief observations can be made at this time:

1. Within the margin of printed-out values (5% change in power), 1-group ANCONMG results agree well with ANCON results.
2. When delayed neutrons were included in the analysis, the peak power and maximum fuel temperature were slightly higher for the 2-group case than for the 1-group case. However, the 1-group results were higher when the delayed neutrons were omitted. Differences were not as large at these reactivity insertions as they are expected to be for larger insertions.

TABLE VII

COMPARISON OF TRANSIENT RESULTS
ANCON AND ANCONMG

Program	No. Groups	Delayed Neutrons Included	Feedback Included	Peak Power (MW)	Time to Peak Power: Transient (sec)	Time to Peak Power: CP (sec)	$(T_f)_{max}$ (°K)	Time to $(T_f)_{max}$: Transient (sec)	Time to $(T_f)_{max}$: CP (sec)
$1.50 Reactivity Insertion									
ANCON		X	X	56.99	3.413	6.249	900.0	26.05	9.592
ANCONMG	1	X	X	56.84	3.409	0.869	900.0	25.26	2.472
ANCONMG	2	X	X	57.00	3.412	457.8	906.5	25.58	3366
ANCON			X	28.92	1.295	10.10	352.7	1.971	15.03
ANCONMG	1		X	29.29	1.312	0.953	352.7	1.974	1.412
ANCONMG	2		X	24.67	1.265	90.1	344.7	1.972	139.8
ANCON		X		0.25[a]	2.140	7.777			
ANCONMG	1	X		↓	2.139	1.122			
ANCONMG	2	X		↓	2.140	227.2			
ANCON				1.95×10^{5}[a]	1.833	15.41			
ANCONMG	1			↓	1.832	0.895			
ANCONMG	2			↓	1.821	69.59			
$0.65 Reactivity Insertion									
ANCON		X	X	1.318	41.57	5.512	570.7	130.53	9.640
ANCONMG	1	X	X	1.367	42.71	0.918	570.7	131.15	3.833
ANCONMG	2	X	X	[b]					
ANCON			X	5.42	2.665	9.123	319.6	4.106	13.56
ANCONMG	1		X	5.65	2.735	1.241	319.6	4.115	1.837
ANCONMG	2		X	4.73	2.668	183.7	315.8	4.129	282.2
ANCON		X		6.0×10^{-6}[a]	2.102	1.701			
ANCONMG	1	X		↓	2.101	0.347			
ANCONMG	2	X		↓	2.101	224.3			
ANCON				1.6×10^{13}[a]	7.133	26.23			
ANCONMG	1			↓	7.134	1.529			
ANCONMG	2			↓	7.174	264.1			

[a] Calculation arbitrarily stopped at this power level.
[b] Peak power not reached after 60.2 min CP time. Extrapolated CP time to peak power = 93.2 min.

3. The 1-group ANCONMG central processor (CP) times were from 2.5 ($0.65 reactivity, delayed neutrons and feedback included) to 17.2 ($1.50 reactivity, no delayed neutrons or feedback) times shorter than the equivalent ANCON CP times. This saving in time was brought about by introducing a variable number of derivatives in the Taylor series in ANCONMG, whereas ANCON has a fixed number of derivatives.
4. The 2-group ANCONMG CP times were from 77.7 ($1.50 reactivity, no delayed neutrons or feedback included) to 6091 ($0.65 reactivity, delayed neutrons and feedback included) times as long as the equivalent 1-group ANCONMG CP times.
5. When delayed neutrons were eliminated from the 2-group analysis, the CP time to peak power was reduced by a factor of 5, the CP time to maximum fuel temperature by a factor of 24.

Direct comparisons between the actual peak powers and maximum fuel temperatures are prohibitively expensive in CP time for 2-group problems that include delayed neutrons. A quicker insight may be gained about multigroup behavior trends, however, from a comparison of the time profiles of the leading edge of the power peak for larger reactivity insertions.

A study was conducted on numerical methods other than continuous analytic continuation. Both the Runge-Kutta and Milne Central Difference Predictor-Corrector methods were tried. However, for stable numerical results to be obtained, the time step size had to be shortened to the point where the resulting CP times were 1.5 to 2.0 times as long as those encountered with ANCONMG.

B. Preparation and Maintenance of Code Packages

1. Application of Synthesis Techniques (B. M. Carmichael)

By synthesis techniques, the number of parameters can be formally reduced in calculational problems. For example, time-dependent one-dimensional solutions to neutron kinetics problems can be obtained by synthesizing the separate space and time solutions, or two-dimensional static solutions to neutron transport problems can be obtained by combining the separate solutions for each of the two space dimensions. In either of these applications, the synthesis method would reduce computing times by more than an order or magnitude.

Multigroup Diffusion Theory. With respect to static neutron diffusion problems, the synthesis is performed with the multigroup diffusion theory Lagrangian

$$L = \sum_g \iint \phi_g^*(x,y)\, H\, \phi_g(x,y)\, dx\, dy. \qquad (1)$$

We consider here a rectangular geometry (x,y), but the method works as well for other two-dimensional geometries. In Eq. 1, if L is varied by varying the adjoint flux ϕ_g^* in group g, the diffusion equation

$$H\phi_g(x,y) = -\nabla \cdot D_g \nabla\phi_g + \sigma_g \phi_g - \sum_{g'} \phi_{g'}\left[\sigma_{g'g} + \frac{\chi_g(\nu\sigma_f)_{g'}}{K}\right] = 0 \qquad (2)$$

is obtained; that is,

$$\delta L(\phi_g^*) = \langle \delta\phi_g^*\, H\delta_g \rangle = 0. \qquad (3)$$

Similarly, a variation of the flux ϕ_g gives

$$\delta L(\phi_g) = \langle \delta\phi_g\, H^*\, \phi_g^* \rangle = 0, \qquad (4)$$

since

$$H^*\, \phi_g^* = 0 \qquad (5)$$

is the equation adjoint to Eq. 2.

One application of Eq. 1 is to the synthesis of two-dimensional diffusion problems. If it is assumed that ϕ_g^* and ϕ_g are separable in x and y,

$$\left.\begin{aligned} \phi_g^*(x,y) &= \phi_{1g}^*(x)\quad \phi_{2g}^*(y) \\ \phi_g(x,y) &= \phi_{1g}(x)\ \phi_{2g}(y) \end{aligned}\right\}, \qquad (6)$$

and variations of Eq. 1 with respect to ϕ_{1g} and ϕ_{1g}^* are taken, one obtains

$$(D_{1g}\, B_{1g}^2 + \sigma_{1g})\, \phi_{1g}^* - \sum_{g'} \phi_{1g}^*\left[\sigma_{1gg'} + \frac{S_{gg'}}{K}\right] - \frac{d}{dx}\left(D_{1g}\, \frac{d\phi_{1g}^*}{dx}\right) = 0 \qquad (7)$$

$$(D_{1g}\, B_{1g}^2 + \sigma_{1g})\, \phi_{1g} - \sum_{g'} \phi_{1g'}\left[\sigma_{1g'g} + \frac{S_{g'g}}{K}\right] - \frac{d}{dx}\left(D_{1g}\, \frac{d\phi_{1g}}{dx}\right) = 0$$

where

$$\left.\begin{aligned} D_{1g}(x) &= \int D_g\, \phi_{2g}\, \phi_{2g}^*\, dy \\ D_{1g}(x)\, B_{1g}^2(x) &= \int D_g\, \frac{d\phi_{2g}}{dy}\, \frac{d\phi_{2g}^*}{dy}\, dy \\ \sigma_{1,g'g}(x) &= \int \phi_{2g}^*\, \phi_{2g'}\, \upsilon_{g'g}\, dy \\ S_{g'g}(x) &= \chi_g \int \phi_{2g}^*\, \phi_{2g'}\, (\nu\sigma_f)_{g'}\, dy \end{aligned}\right\}. \qquad (8)$$

Equations in y exactly analogous to Eqs. 7 and 8 are obtained by taking variations with respect to ϕ_{2g} and ϕ_{2g}^*.

Equations 7 are the regular and adjoint one-dimensional diffusion theory equations in x. The procedure for using these equations would be to solve a problem in y first using, for example, DTF with the buckling option.[8] The y solutions are substituted into Eqs. 8 to obtain the parameters needed for input to Eqs. 7; for this, the parameters would be input to a DTF problem set up to solve the x dimension case. Parameters derived from the latter

solution would be substituted back into the y case, and so on. This is a lengthy procedure requiring automation.

Multigroup Transport Theory. A procedure based on diffusion theory might be poorly suited to some problems, particularly small fast assemblies. For such cases, the transport Lagrangian

$$L = \iiint \Psi_g^*(\underset{\sim}{r},\underset{\sim}{\Omega})\, H\Psi_g(\underset{\sim}{r},\underset{\sim}{\Omega}')\, d\underset{\sim}{\Omega}\, d\underset{\sim}{\Omega}'\, d\underset{\sim}{r} \qquad (9)$$

should give better results where

$$H\Psi_g = [\nabla \cdot \underset{\sim}{\Omega}'\, \Psi_g(\underset{\sim}{r},\underset{\sim}{\Omega}') + \sigma_g\, \Psi_g(\underset{\sim}{r},\underset{\sim}{\Omega}')]\, \delta(\underset{\sim}{\Omega}' - \underset{\sim}{\Omega})$$

$$- \sum_{g'} \Psi_{g'}\left(\underset{\sim}{r},\underset{\sim}{\Omega}'\right)\left(\sigma_{g'g} + \frac{\chi_g(\nu\sigma_f)_{g'}}{K}\right) = 0 \qquad (10)$$

is the transport equation in terms of the angular fluxes Ψ_g and Ψ_g^*. As in the diffusion case,

$$\delta L(\Psi_g, \Psi_g^*) = 0 \,. \qquad (11)$$

However, if one attempts to separate the variables as in the diffusion case, that is, if one assumes, for example, that

$$\Psi_g(x,y,\Omega_x,\Omega_y) = \Psi_{1g}(x,\Omega_x)\, \Psi_{2g}(y,\Omega_y), \qquad (12)$$

then the variational principle does not yield clean one-dimensional transport equations. Even the current approximation

$$\Psi_{1g}(x,\Omega_x) = \phi_{1g}(x) + 3\,\Omega_x\, J_{1g}(x), \qquad (13)$$

which is a near diffusion theory assumption, does not appear to provide a tractable approach. Solutions to this problem have not been found in the literature. Further study is indicated.

2. Calculation of Central Reactivity Worths (M. E. Battat)

Certain inconsistencies have been noted in the results of calculations to determine the central reactivity worth of ^{239}Pu in JEZEBEL. As an example, the finite-sample (0.7268-cm radius) worth calculated by the DTF-IV code[8] (eigenvalue difference method) was slightly larger than the small-sample (0.1454-cm radius) worth calculated by the DAC code (perturbation method). Experimentally, the finite-sample worth is about 8% less than the small-sample worth.

To investigate this anomaly, the original DTF-IV S_8 calculations were repeated with finer mesh spacing (10 instead of 5) in the sample region; in addition, the problems were rerun with the S_{16} option. A summary of the DTF-IV and DAC problems with the S_8 and S_{16} options is given in Table VIII.

TABLE VIII

^{239}Pu CENTRAL WORTH IN JEZEBEL

Problem	Theory	S_n	k_{eff}	Core Radius (cm)	Material in Center	Δk/g-atom
DTF-IV						
01058	REG	8	critical	6.2807	Fuel	
021868	REG	16		6.3023		
01048	ADJ	8		6.2807		
021968	ADJ	16		6.3023		
01038	REG	8		6.3044	Void	
022168	REG	16		6.3250		
12287	ADJ	8		6.3044		
022268	ADJ	16		6.3250		
12317	REG	8	1.003959	6.3044	^{239}Pu	0.03090
022368	REG	16	1.003861	6.3250		0.03014
11197	ADJ	8	1.003959	6.3044		0.03090
022468	ADJ	16	1.003860	6.3250		0.03013
DAC (small sample)						
01048 & 01058		8		6.2807	Fuel	0.03122
021868 & 021968		16		6.3023		0.03119
DAC (0.7268 sample)						
12287 & 12317		8		6.3044	Void	0.02869
022268 & 022368		16		6.3230		0.02870

Although the analysis of the results is not yet complete, it can be seen that the ^{239}Pu worth was reduced by 2.5% in going from S_8 to S_{16}; however, the critical mass was increased by 1%. In contrast, the DAC results did not seem to change significantly in going from S_8 to S_{16}. Examination of the data is still in progress.

3. One-Dimensional Perturbation Code (B. M. Carmichael, R. L. Cubitt)

The one-dimensional version of the DAC perturbation code, DAC1, is being written in the same

format as the one-dimensional S_n code DTF.[8] Accordingly, the input format is the same as in DTF, the variable dimension scheme from DTF is used, and the options in DTF applicable to perturbation theory are preserved.

Input for DAC1 consists of the unmodified input deck to DTF, flux dumps from regular and adjoint DTF k-eigenvalue problems for the nuclear system under study, and specification of perturbations.

The entire code has been written; the input section, the calculation of the effective delayed neutron fraction, the neutron lifetime calculation, and the buckling perturbation option have been debugged. The calculation of the delayed neutron fraction has been generalized to permit calculation of an arbitrary mixture of delayed neutron emitters.

The buckling perturbation was added recently. In DTF, the buckling parameters introduce fictitious absorption in the one-dimensional calculation which accounts approximately for neutron leakage in directions transverse to the specified dimension. The buckling corrections are calculated from the extrapolated heights or radii in the directions transverse to those stipulated in the DTF input. DAC1 calculates the reactivity resulting from a perturbation of the extrapolated dimensions.

The remaining perturbation sections of the code are being debugged. These routines will provide reactivity estimates for arbitrary perturbations of the atom densities, dimensions, and microscopic cross sections of the nuclear system.

REFERENCES

1. M. K. Drake et al., "Neutron and Gamma-Ray Production Cross Sections for Sodium, Magnesium, Chlorine, Potassium, and Calcium," NDL-TR-89, GA-7829, General Atomic (1967).

2. K. Parker, "The Aldermaston Nuclear Data Library as of May 1963," AWRE-O-70/63, UKAEA (1963).

3. Donald J. Dudziak (ed.), "ENDF/B Format Requirements for Shielding Applications," LA-3801, Los Alamos Scientific Laboratory (1967).

4. K. F. Hansen and S. R. Johnson, "GAKIN, A One-Dimensional Multigroup Kinetics Code," GA-7543, General Dynamics (1967).

5. S. R. Johnson, "WIGL2 Modified for Use on the UNIVAC-1100. A Supplement to the Westinghouse Report Number WAPD-TM-532," GAMD-7545, General Dynamics (1967).

6. J. C. Vigil, "Solution of the Nonlinear Reactor Kinetics Equations by Continuous Analytic Continuation," LA-3518, Los Alamos Scientific Laboratory (1966).

   J. C. Vigil, Nucl. Sci. Eng. 29, 392 (1967).

7. G. Robert Keepin, Physics of Nuclear Kinetics, Addison-Wesley, Reading, Mass. (1965), 90.

8. K. D. Lathrop, "DTF-IV, A FORTRAN-IV Program for Solving the Multigroup Transport Equation with Anisotropic Scattering," LA-3373, Los Alamos Scientific Laboratory (1965).

PROJECT 822

EXAMINATION OF FAST REACTOR FUELS

Person in Charge: R. D. Baker
Principal Investigators: J. W. Schulte
J. A. Leary
C. F. Metz

I. INTRODUCTION

This project is directed toward the examination and comparison of the effects of neutron irradiation on LMFBR Program fuel materials. Irradiated materials will be examined as requested by the Fuels and Materials Branch of DRD & T.

II. FUEL CAPSULE HANDLING CAPABILITY

(P. J. Peterson)

Re-evaluation of the cask design for shipping irradiated capsules from EBR-II to LASL is being done, and an engineering analysis of its performance under the hypothetical accident conditions of Chapter 0529 of the AEC Manual is being undertaken. Procurement of the cask will be delayed until FY 1969.

III. INERT ATMOSPHERE BOXES

(M. D. Keehn, R. F. Velkinburg)

Testing of the Ar purification unit in conjunction with an alpha containment box to be used in-cell has been completed. With a 1 CFH Ar purge through the volume between the manipulators and booting, the discharge from the box was maintained at ~ 1 ppm H_2O and ~ 2 ppm O_2. To simulate damage to the booting a 1/8 in. diam hole was made in the boot and, with the Ar purge of the boot increased to 20 CFH, no adverse effects were notod. Moderate manipulator activity produced no change. It is to be emphasized that these tests were performed under ideal conditions and are not necessarily representative of the purity that can be maintained in real operation.

Controlled and measured air leaks were introduced in the system to determine the effectiveness of the purification unit. It was found that with an air (~ 50% relative humidity) leak rate of 100 cc/min, H_2O concentrations were kept at < 5 ppm, but O_2 levels rose to >100 ppm. This deficiency has been reported to the supplier for possible corrective recommendations.

IV. IN-CELL EQUIPMENT

(E. L. Ekberg, F. J. Fitzgibbon, G. H. Mottaz, P. J. Peterson, T. Romanik, J. R. Trujillo)

Na Distillation

The unit for distilling Na from irradiated fuel pellets has been fabricated and is currently being tested to ascertain the optimum vacuum and temperature conditions for quantitative Na removal.

Gamma Scanning

The new unit for handling fuel capsules up to ~ 40 in. long has been designed, and commercially available components have been ordered. Fabrication will proceed in the near future.

Fission Gas Sampling

Development of the new system for puncturing the clad of irradiated capsules, measuring gas pressure and sampling for fission gas analysis is currently in progress.

Density Measurement

Density determination of mock-up pellets generating 0.5 watts of heat in a volume of ~ 0.3 cc has shown density errors of ~ 0.4% due to the thermal currents in

the immersing media. Work is continuing on methods of reducing this error.

De-Canning Saw

As a back-up for cladding removal by stripping, a saw for slitting and sectioning of irradiated capsules has been fabricated. The unit is in the process of being tested.

Technique For Removing EBR-II Driver Fuel From Cladding

A furnace, using heating tapes, was fabricated for the purpose of removing the fuel pin as an integral unit from the clad.

The technique employed is as follows: the fuel element is sectioned with a tubing cutter at the lower end near the plug and at the upper end near the restrainer. The upper end of the section containing the fuel pin is then opened up beyond its original diameter with a flaring tool. The flared end is inverted in the furnace, and a collet is tightened on the opposite end. After evacuating the furnace assembly it is heated to ~ 175°C, a rod (extending through the furnace cap) is forced down on the fuel by the use of manipulators. The fuel is ejected from the clad into a receiving tube which is the lower part of the furnace assembly. After cooling the furnace and venting, the entire assembly is rinsed with Dowanol EB to dissolve the residual Na, and the clad and fuel pin are removed.

To date 3 unirradiated pins and 2 irradiated pins have been removed in this manner. Fuel with increased swelling is obviously more difficult to remove. This technique, however, permits: taking diametral measurements on the full length of fuel pin; viewing of the entire length of an intact pin; and preserving the cladding for such measurements as tensile tests on tubes.

V. DIFFERENTIAL THERMAL ANALYSIS

(D. B. Court)

Fabrication of all components for the differential thermal analysis system has been completed. Installation of the induction heating generator and oscillator is under way, and the in-box furnace components are installed. The alpha box is 90% prepared for in-cell installation.

VI. HEAT CONTENT MEASUREMENT

(C. E. Frantz)

Design of the isothermal drop calorimeter has been completed. Fabrication of the block portion is about 80% complete. Materials are being procured for the furnace. An instrument console for the calorimeter is in the initial stages of fabrication. Installation of the vacuum pumps and electrical transformers for the calorimeter is in progress. Design of the power leads from the transformers to the furnace has been completed. Various layout designs of utilities required for the calorimeter have been drawn.

Design of the welding fixture for sealing tungsten capsules used in the calorimeter has been completed, and the fixture has been fabricated.

VII. ANALYTICAL CHEMISTRY

(O. R. Simi, J. H. Dahlby, C. S. MacDougall, T. K. Marshall, G. R. Waterbury)

The Determination of Free (Uncombined) Carbon in Irradiated Carbide Fuels

In adapting a method (Rpt. LA-3603, 1966) for remote manipulation, a compact fused-silica furnace, for igniting the separated free C, coupled with a Ni furnace filled with CuO was tested by analysis of twelve portions of a UC sample for total and free C. Average values of 9.32% total C and 0.91% free C were obtained. The total C content is in agreement with an average of 90.1% obtained for U in this sample. Operation of the furnace using manipulators was found to be satisfactory. Installation in the hot cell has started.

Dissolution of Uranium Fuels Containing Ru (U Fissium)

Several samples of unirradiated U-fissium alloy were dissolved in a HCl-HNO_3-$HClO_4$ mixture in a dissolver designed for hot cell use. The apparatus consists of a closed dissolver pot connected to a water-cooled NaOH trap to collect volatile Ru. Samples ranging between 0.5 and 1 g were dissolved without visible residue remaining, and the recovery of Ru was 100%. The dissolver was installed in a hot cell and applied successfully to dissolution of irradiated fuel alloys.

Determination of Oxygen in Irradiated Reactor Fuels

A fused-silica furnace designed for inert-gas-fusion measurement of O_2 in irradiated fuels was tested under simulated hot cell conditions. Plans for installation of the furnace in a hot cell were made, and installation of the induction heater and other ancillary equipment was started. Some delays are anticipated because an inert atmosphere enclosure for sample preparation is not completed.

Adaptation of Emission Spectrographic Methods to the Analysis of Irradiated Materials

(a) Analysis of Irradiated U-Pu Fuels

Unirradiated UC_2 is being used as a stand-in material for adapting a carrier-distillation method to the analysis of irradiated U-Pu fuel by remote manipulation in a hot cell. Individual steps such as weighing and crushing the sample, igniting to the oxide, mixing sample with 4% Ga_2O_3 as a carrier, loading the electrodes and exciting the sample with a d.c. arc have been remotized. Twenty-one impurity elements may be determined in concentrations varying from the limit of detection (0.3 to 30 ppm depending on the element) to an upper limit of about 300 ppm.

(b) Analysis of Sodium Metal Containing Fission Products

This method is being adapted to hot cell operation. It involves weighing the sample, dissolving in butanol, converting to NaCl, by addition of HCl, evaporating to dryness, mixing with graphite and d.c. arc excitation. The limits of detection obtained with standards arced in the hot cell are shown in Table I. Li and K will be added to the list.

Table I

Tentative Limits of Detection for Impurity Elements in Sodium

Element	Limit of Detection, ppm	Element	Limit of Detection, ppm
Be	0.8	Ni	3
B	8	Cu	3
Mg	3	Zn	300
Al	3	Sr	0.8
Si	3	Mo	0.8
Ca	0.8	Ag	0.8
Ti	3	Cd	30
V	0.8	Sn	0.8
Cr	0.8	Ba	30
Mn	0.8	Pb	3
Fe	0.8	Bi	3
Co	8		

VIII. EXAMINATION OF UNIRRADIATED FUELS

Plastic Deformation
(M. Tokar, A. L. Gonzales)

Preliminary testing of 1/2 in. diam x 1/2 in. tall cylindrical specimens of UC has been started with the new instrument. The press and furnace have been enclosed for plutonium work. Maximum temperatures and pressures were 1400°C and 7000 psi, respectively, with the original arrangement of the 15 KVA motor-generator set. Leads from this power supply are being modified in order to raise the operating temperature to at least 1800°C.

Thermal Conductivity
(K. W. R. Johnson)

The 3M Model TC-200 comparative type thermal conductivity apparatus has been modified for use on smaller plutonium specimens.

Thermal conductivity calibration measurements were continued using a 1/2 in. diam x 1/2 in. long meter-specimen-meter assembly fabricated of Inconel 702. In anticipation of compatibility problems associated with nuclear fuels and the components of the apparatus at high temperature, an attempt was made to make measurements in vacuum. With the existing equipment, good thermal balance could not be obtained when either ceramic packing or radiation shields were used between the conductivity stock and the guard. In an inert atmosphere, with radiation shields instead of ceramic insulation and using matched guarding the measurements at 200°C were within the ± 10% accuracy specified for the apparatus. At 500°C the accuracy exceeded 10%, but acceptable accuracy was obtained at 500 and 750°C by using linear guarding. By adjusting the temperature profile of the guard to minimize the interface temperature gradients between meters and

specimen, accuracies at 677 and 981°C were 7.2 and 6%, respectively.

A specimen of AAQ graphite has been substituted for the Inconel specimen to test the reliability of the measuring procedure in a different thermal conductivity range.

The glovebox for housing the thermal conductivity apparatus has been received and is being installed.

Hot Hardness
(A. L. Gonzales)

The instrument has been installed in a glovebox, and is essentially ready for use.

Vacuum Cathodic Etching
(K. A. Johnson, A. L. Gonzales)

A minor design change was made to the glovebox enclosure to accommodate high voltage feed-throughs. The instrument is essentially ready for use.

IX. EXAMINATION OF EBR-II DRIVER FUEL
(K. A. Johnson, J. W. Schulte, G. R. Waterbury)

At the request of the Division of Reactor Development and Technology, LASL will do an extensive study on 6 irradiated EBR-II Driver Fuel Rods.

The results obtained to date are given below.

Fuel Element

A. Measurements of Physical Properties

B. Stereo-viewing and Macro-photography

All six irradiated and five unirradiated elements were visually examined. The only notable feature was a slight discoloration (golden brown) on all the elements. The elements with the most prominent stain SL 42-17 (irradiated) and SL 49-60 (unirradiated) were selected for an attempt to identify the stain by chemical analyses.

C. Chemical Analyses of Surface Material in Discolored Areas on Stainless Steel Clad and Wires

Discolored surface areas on spacer wires or cladding of three fuel elements were leached in succession with alcohol-acetone and then twice with a dilute HCl-HNO_3 solution. The first acid leach removed the discoloration and the second dissolved some of the substrate material to provide a reference solution. Emission spectrochemical determinations of the major constituents were made on each of the leach solutions. The total quantities of material found in each of the first two leaches of each sample were small, ranging from 0.8 to 44.4 μg. Iron, chromium, and nickel, which are constituents of the stainless steel, were the main solutes in the acid leach solutions. Submicrogram quantities were found of surface contaminants such as Cu, Y, Pb, Mn, Al, and Ca. Oxygen, which might contribute to the surface discoloration, could not be measured because of the nature of the

Table II

Measured Physical Properties

Element	Radiation,[1] R/hr at 1 m	Weight, g	Max. Surface Temp., °C[2]	Dimensions in inches Diam. (± 0.0002 in.) Max.	Min.	Length (±1/32 in.)	Bow,[3] in.
4015-56 (Irrad.)	28	84.82	30.6	0.1750	0.1744	18 1/16	0.080
SL 38-16 (Irrad.)	29	84.64	29.2	0.1754	0.1750	18 1/16	0.035
4088-100 (Irrad.)	30	84.49	29.9	0.1749	0.1743	18 1/16	0.018
4087-53 (Irrad.)	32.5	84.80	29.6	0.1746	0.1742	18 1/16	0.011
4057-84 (Irrad.)	26	84.07	30.7	0.1736	0.1732	18 1/16	0.038
SL 42-17 (Irrad.)	28	84.42	30.0	0.1752	0.1748	18 3/32	0.019
SL 49-60	--	84.81	--	--	--	18 1/16	--
0459-14	--	83.54	--	--	--	18 1/16	--
0121 H-05	--	--	--	0.1735	0.1729	--	0.014
0121 H-23	--	--	--	0.1739	0.1735	--	0.055
0121 H-27	--	--	--	0.1735	0.1728	--	0.027

[1] Swipes showed no α contamination and 4-50 mr/hr β-γ contamination.

[2] Temperature of hot cell was 29.0°C.

[3] Bow measurements are to ± 0.005 in., but flexibility of the fuel elements makes the tolerance accuracy doubtful. Some bow may have been induced by handling.

sample. It was difficult to evaluate the significance of the metallic contaminants which might have been introduced onto the surface during the many handling operations.

D. Gamma Scanning
(Dale M. Holm, K-1)

A series of gamma scans with 4 keV energy and good spatial resolution have been made on EBR-II driver fuel pins. Twenty-two gamma-ray lines were observed and analyzed from the spectra taken at different positions. Table III shows the energies of the lines, the isotope identification and the method of production. Although

Table III

Gamma-ray Energies Observed in EBR-II Driver Fuel Element (No. 4087-53), Their Identification, and Method of Production

Gamma-ray Energy (keV)	Isotope	Reaction
2186	^{144}Pr	Fission Product
1490	^{144}Pr	" "
1332	^{60}Co	$^{59}Co(n,\gamma)^{60}Co$
1173	^{60}Co	" "
1050	^{106}Rh	Fission Product
834	^{54}Mn	$^{54}Fe(n,p)^{54}Mn$
810	^{58}Co	$^{58}Ni(n,p)^{58}Co$
765	^{95}Nb	Fission Product
757	^{95}Zr	" "
724	^{95}Zr	" "
695	^{144}Pr	" "
662	^{137}Cs	" "
620	^{106}Rh	" "
512	^{106}Rh	" "
512	^{58}Co	$^{58}Ni(n,p)^{58}Co$
497	^{103}Ru	Fission Product
144.7	^{141}Ce	" "
133.5	^{144}Co	" "
116	Unidentified	Unidentified
112	"	"
100	"	"
97	"	"

all of the data has not been interpreted, preliminary results indicate that no migration of fission products occurred in the fuel elements.

There is a marked difference in the distribution of stainless steel activation products as compared to the fission products. The activity from fission products in the median plane is 30% higher than at the ends of the fuel, whereas the fast (> 2 MeV) neutron (n,p) activation products (^{54}Mn and ^{58}Co) are 260% higher in the median plane than at the ends of the fuel. Conversely, the thermal neutron activation product (^{60}Co) is not detected in the fueled region but is seen in the nonfueled region.

Since no (n,α) reaction products from stainless steel were observed, it is presumed that they will not be detectable by gross gamma counting of the fuel elements. However, since both the (n,α) and the (n,p) reactions are from the high energy component of fission neutrons, it should be possible to deduce the number of (n,α) reactions in the stainless steel.

E. Nondestructive Tests
(Group GMX-1)

1. Beta-Gamma Autoradiographs

The six irradiated elements were autoradiographed; the dark images obtained were then x-ray radiographed at a low energy level. The resulting radiographs were traced with a microdensitometer. The maximum change in film density of the fuel element images was about 2.2%.

This method is not particularly productive of information as applied to this particular type of fuel element.

2. Eddy Current Measurements

Eddy current measurements were made on the elements at a frequency of 250 K Hz with the results as shown in Table IV. The values in Table IV have not yet been correlated with any particular features of the element; however, low conductivity indications may show Na voids.

Table IV

Locations of Conductivity Changes

Element	Distance from Top of Fuel Element, in Inches ± 0.2 Inches						
4015-56(Irrad.)	4.6*	5.6	11.5	13.5			
SL38-16(Irrad.)	1.1	1.75	3.9*	6.6	7.75	12.1*	
	13.2	13.8	14.4*	15.0*	15.5	15.75	16.4
4088-100(Irrad.)	1.13	2.6	3.6	6.6	14.2	14.3	
	14.9	16.2					
4087-53(Irrad.)	4.5	5.9	9.4	13.5			
4057-84(Irrad.)	2.0	6.3	9.25	11.8	12.4	13.9	14.3
SL42-17(Irrad.)	2.0*	3.7	9.3*	10.1 to	11.0*	11.75	12.3
	12.8	16.1					
0121H-05	4.5	6.9	7.7	11.3 to	11.7	12.4 to	12.9
	13.4 to	13.9					
0121H-23	2.1	3.0	3.4 to 3.7	6 to 7.5	10.5		
0121H-27	5.3	6.2	10.5 to 10.9	15.2			

*High conductivity points, all others are low conductivity points.

3. X-ray Radiography

Results of radiographic inspection of 9 elements are as follows:

Element	
4015-56(Irrad.)	Five voids, 10 to 30 mils diam located in the fuel pin between 1 and 2 inches from the bottom of the capsule.
SL38-16(Irrad.)	No voids detected.
4088-100(Irrad.)	Two voids in the fuel pin, about 10 mils diam, 5.2 and 5.6 inches from the top end of the element.
4087-53(Irrad.)	No voids detected.
4057-84(Irrad.)	No voids detected.
SL42-17(Irrad.)	No voids detected.
0121H-05	Voids in the fuel pin from the top to 6.8 inches from the bottom, all in center of pin.
0121H-23	Possible incomplete fusion in weld at top end. Voids all along the center of the fuel pin.
0121H-27	No voids detected.

4. Sodium Level Measurements

Sodium levels in the elements, as measured from the top of each element, were determined to be as follows:

Table V

Measured Sodium Levels, in Inches

Element	By X ray Radiography	By Eddy Current ± 0.125 in.
4015-56(Irrad.)	1.03	1.00
SL38-16(Irrad.)	0.84	0.75
4088-100(Irrad.)	2.55	2.75
4087-53(Irrad.)	1.82	1.75
4057-84(Irrad.)	2.45	2.25
SL42-17(Irrad.)	1.46	1.13
0121H-05*	2.81	
0121H-23*	2.40	
0121H-27*	2.81	

*These elements were rejected by ANL because the Na levels did not conform to specifications.

5. Infrared Radiometry

One unirradiated element was inspected by this method, and preliminary indications are that this technique may be useful in detecting Na levels.

Components

A. Clad

1. Chemical Analyses

The bottom tip and one section of clad from each of two unirradiated fuel elements were analyzed by a microcombustion method for C. The tips contained 60 to 65 ppm, and the clad from elements SL49-60 and 0121H-05 contained 80-180 ppm, respectively. These C values were within the maximum specified in the composition requirements of ASTM-A-240-63 for type 304 L stainless steel and in the Product Specification for the EBR-II Driver Fuel Elements, FCF-1. Emission spectrographic analyses for metallic constituents and additional carbon determinations are in progress.

2. Metallography and Autoradiography

Sections of the clad from element 4007-53 (irradiated) were mounted and metallographic examinations are in progress. Alpha and beta-gamma autoradiographs have been made. With exposures of up to 40 min, they show no detectable images. Longer exposures will be tried.

3. Tensile Tests

Preliminary results of tensile tests on sections of clad are given in Table VI.

Table VI

Tensile Test Results

Clad from Element	Clad Length, in.	Head Speed, in./min.	Yield Point*	Ultimate Point*
4087-53(Irrad.)	5	0.5	426 lbs	519 lbs
SL49-60	3-1/2	0.05 to 0.5	162 lbs	462 lbs
0121H-05	6	0.5	225 lbs	444 lbs
0121H-27	3-1/2	0.5	225 lbs	432 lbs

*Strengths are reported direct, not as psi.

The above results indicate a probable increase in both yield and ultimate strengths in the clad as a result of the irradiation. Metallography may pinpoint the strengthening mechanism.

B. Fuel Pins

1. Stereo-Viewing

Three unirradiated and one irradiated fuel pin were examined; the only notable feature was a few shallow depressions on the irradiated rod 4087-53.

These depressions may have been produced during the removal of the fuel from the clad, as evidenced by flakes found in the Na and the disassembly equipment.

2. Measurements

Table VII

Measured Physical Properties

Element	Weight, g	Immersion Density, g/cc, ±0.16% Near Top	Immersion Density, g/cc, ±0.16% Near Bottom	Dimensions, in. Diam(±0.0002 in.) Max.	Dimensions, in. Diam(±0.0002 in.) Min.	Length, in. (±0.03 in.)
4088-100(Irrad.)	64.95	---	---	0.1479[a]	0.1450	13.56
4087-53(Irrad.)	64.90	15.77	16.63	0.1530	0.1488	13.81[b]
SL49-60	---	18.06	18.03	---	---	---
0121H-05	---	17.91	17.97	---	---	---
0121H-27	63.79[c]	17.95	17.94	0.1438	0.1413	---

[a]Diameter of pre-irradiation pin is ~0.144 in.

[b]Pre-irradiation length of this fuel pin was 13.499 in.

[c]Weight of this fuel pin, as reported by ANL Idaho, was 63.81 g.

The weight of fuel pin 4087-53 is 0.16 g lower than the pre-irradiation weight (65.06 g), as reported by ANL Idaho. This difference may be attributed to the dislodging of small chips during the removal of fuel from clad.

Surface temperatures measured for two irradiated fuel pins were within 1°C of the hot cell temperature (31°C).

3. Chemical and Isotopic Analyses

Concentrations of some alloying elements and impurities were determined in two fuel pins by spectrophotometric and radiochemical methods, and the isotopic composition of the uranium was measured mass spectrometrically. These determinations were made on aliquots of solutions prepared by dissolving 1-g samples taken from the top, middle, and bottom of the fuel pins. Solid samples from the middle of each rod were analyzed by an inert gas fusion method for O_2 and a microcombustion method for C. The results obtained to date (Table VIII) are within the concentration ranges listed in Product Specification for the EBR-II Driver Fuel Elements, FCF-1, with the exception of the slightly higher concentrations of 2.76% for Mo and 2.19% for Ru in the top sample of fuel pin SL-49-60, and the slightly lower isotopic concentration for ^{235}U. Emission spectrographic determinations of impurities in the samples from the middle of each pin and controlled-potential coulometric titrations of the U in each sample are in progress.

Samples from irradiated fuel pin 4087-53 are dissolved and analyses are started.

Table VIII

Chemical Analyses of EBR-II Driver Fuel Pins

Element	Specified Concentration[a]	Concentrations Pin SL49-60 Top	Pin SL49-60 Middle	Pin SL49-60 Bottom	Pin 0121H-05 Top	Pin 0121H-05 Middle	Pin 0121H-05 Bottom
Mo	2.40 ± 0.17%	2.76%	2.49%	2.51%	2.32%	2.32%	2.32%
Ru	1.96 ± 0.16%	2.19%	1.97%	1.96%	2.00%	1.99%	2.00%
Rh	0.28 ± 0.05%	0.29%	0.27%	0.27%			
Pd	0.19 ± 0.04%	0.21%	0.20%	0.19%	0.19%	0.20%	0.19%
Zr	0.10 ± 0.03%	0.079%	0.066%	0.069%			
Th	< 100 ppm	7 ppm	9 ppm	9 ppm			
Pu	--	9.6 ppm	10 ppm	9.6 ppm	< 1 ppm	< 1 ppm	< 1.1 ppm
O	< 200 ppm		80 ppm			90 ppm	
C	< 400 ppm		165 ppm			400 ppm	
U	95.0 ± 1.0%						
^{235}U	52.18 ± 0.50%	51.99%	51.99%				
^{234}U, ^{236}U, ^{238}U	47.82 ± 0.50%	48.00%	48.00%				
^{234}U, ^{236}U	< 1.0%	< 1.0%	< 1.0%				

[a]Product Specifications for the EBR-II Driver Fuel Elements, FCF-1

4. Metallography and Autoradiography

Metallography is in progress on top, middle and bottom sections of pins No. 4087-53 (irradiated, SL49-60, 0121H-05 and 0121H-27. Preliminary alpha and beta-gamma autoradiographs have been made to determine exposure time and to check hot cell techniques.

5. Retained Fission Gas Measurement

Identification and measurements will be made on fission gases retained in the fuel by complete dissolution of 1 in. sections. The work is currently in progress.

C. Sodium

1. Chemical Analyses

Metallic impurities in the Na from two capsules were determined by an emission spectrographic method. The Na was leached with butanol from the top section of the clad of element SL49-60, and two small samples of metallic Na were removed with a spatula from the clad about 3.4 inches below the top end of element 0121H-27. Hydrochloric acid was added to each sample and the butanol was evaporated to prepare the samples for analysis. The results (Table IX) show that the Na removed mechanically from the element was more pure than the Na leached from element SL49-60 by butanol. The higher impurity concentrations obtained for the leached sample could be the result of foreign

material either on the cladding or in the Na. Reagent blank determinations showed that the reagents were not contaminated. Unfortunately, it was not possible to remove Na samples mechanically from the irradiated elements, but great care was exercised in cleaning the outside of the cladding prior to leaching of the sodium with Dowanol. Emission spectrographic analyses of these Na solutions are in progress.

Table IX

Concentrations of Impurities in Sodium

Element	Specified[a] Maximum, ppm	Concentrations, ppm in Na from SL49-60	0121H-27
Ag	20	< 0.8	< 0.8
Au	30	60	< 3
B	5	12	< 3
Ca	10	200	10
Cd	20	3	< 3
In	30	< 3	< 3
K	1000	120	125
Li	20	< 0.8	< 0.8

[a]Product Specifications for the EBR-II Driver Fuel Elements, FCF-1

PROJECT 824

FAST REACTOR METALLIC FUEL STUDIES

Persons in Charge: R. D. Baker
D. B. Hall

Principal Investigators: W. J. Maraman
R. H. Perkins

I. INTRODUCTION

The objective of this program is the development of metal fuels for fast reactor application. The primary effort is placed on preparation and fabrication development of the Pu-U-Zr alloys. Supporting effort is directed toward areas of physics and system evaluation, determination of physical and chemical properties, and fuel-cladding interactions.

II. FUEL PREPARATION AND FABRICATION
(D. R. Harbur)

A. General

The initial goals of this project are to prepare high purity, homogeneous U-15 w/o Pu - 10 to 15 w/o Zr alloys, to fabricate these alloys into fuel pins of the EBR-II size and to fully characterize these pins. Present efforts are being directed toward the preparation of a high purity, homogeneous alloy. Consideration is also being given to several fabrication methods and to the procurement of fabrication equipment.

B. Current Results

Two methods are being evaluated for the preparation of high purity, homogeneous U-15 w/o Pu-10 to 15 w/o Zr alloys: induction melting in conventional crucibles and in "cold crucibles." Induction melting of the alloying materials inside of a graphite crucible with a non-reactive coating offers the advantage of being able to prepare and cast homogeneous alloys in a one-step operation.

Preliminary data now indicates that a homogeneous ternary alloy may be prepared at 1400°C in less than 0.5 hr provided the melt is mechanically stirred and a U-Zr binary is used with Pu. The binary was prepared from high purity U and crystal bar Zr using repetitious arc meltings. (The O content was held to 70 ppm by weight.)

The reactivity of crucible materials and for crucible coatings with these ternary alloys at 1400°C for short times is being studied. Oxidized Ta melting crucibles, which are routinely used for most Pu alloys, were severely attacked by both a U-15 w/o Zr binary and a U-15 w/o Pu-10 w/o Zr ternary. Flame-sprayed coatings of W, Mo and TaC were badly wetted by the ternary, whereas ZrO_2 and Y_2O_3 were not. However, the ZrO_2 coating was darkened, which indicated O depletion. A quantitative evaluation of ZrO_2 and Y_2O_3 coatings is being conducted. In conjunction with flame-sprayed coatings of ZrO_2 and Y_2O_3, colloidal suspensions of these two ceramics have been ordered from the Acheson Colloids Co. Coatings made from colloidal suspensions are readily applied and have a high adhesive strength.

In the cold crucible technique the ternary alloy is prepared by melting and stirring inside of a water-cooled metallic crucible. In this method there is always a frozen alloy skin next to the water-cooled crucible which prevents pickup of impurities from the crucible. Homogeneous U-15 w/o Zr alloys have been prepared on the wall of a horizontally positioned, water-cooled Cu heat concentrator. (The concentration of Cu in the binary was 13 ppm by weight.) A heat concentrator unit has been installed in a Pu glove box and several 65 g batches

of U-15 w/o - 12.7 w/o Zr alloy have been prepared. Analytical results on these alloys are pending. The heat concentrator is being redesigned to increase the volume of metal contained. These units are powered by a 25 KW radio-frequency unit. An alternate method being studied involves the partial levitation and stirring of a 350 g or larger charge, inside of a thin, water-cooled Ta cone. In this case the charge is heated by the output from a motor-generator set. (This approach offers the added possibility of being able to cast the alloy directly.) In connection with all of the above studies, carefully selected stocks of characterized feed materials have now been obtained. A tentative correlation between hardness and composition of the U-Zr binary has been established.

Casting studies of the ternary are yet to be instituted. Since it may not be feasible to gravity cast rods to the EBR-II size, both extrusion and swaging are to be investigated. The design of a high temperature extrusion die and press is nearing completion. A Fenn swaging machine has been purchased and its enclosure inside of a glove box is being considered.

OTHER ADVANCED SYSTEMS - RESEARCH AND DEVELOPMENT

Person in Charge: D. B. Hall
Principal Investigators: R. H. Perkins
E. O. Swickard

I. AQUEOUS NEUTRON SOURCE
(B. J. Thamer, M. E. Battat)

A. General

One of the more serious problems implicit in the concept of a Liquid Jet Super Flux Reactor[1] is the possible precipitation of uranium peroxide from the aqueous fuel. Such precipitation could cause hot spots on solid surfaces or give problems in the control of the reactor. The reaction of radiolytically produced H_2O_2 with aqueous UO_2SO_4, for example, is nominally

$$UO_2SO_4 + H_2O_2 = UO_4\downarrow + H_2SO_4.$$

This reaction is important below 200°C, i.e. at the temperatures of the LJSFR as presently conceived. At temperatures higher than 200°C the danger from equilibrium would be much reduced because of the nearly instantaneous decomposition of the radiolytic H_2O_2. However, such high temperatures would entail an undesirably high vapor pressure of the solution; hence, temperatures below 200°C are favored. The recombination of radiolytic hydrogen and oxygen could be accomplished with a catalytic recombiner of plantinized alumina.[2]

B. Current Results

1. Fuel Chemistry

Recent studies were concerned with determining the conditions under which UO_4 would precipitate from a UO_2SO_4 solution. Data[3] are available for estimating the H_2O_2 concentration that would be generated for a given amount of fission energy as a unit of the fuel passed through the critical region of a LJSFR. Although the fuel might contain copper and iron salts to decompose H_2O_2, such decomposition would be slight during the approximately 10^{-2} second of transit across the critical region. Table I contains experimental determinations of H_2O_2 solubilities for two fuel compositions. The first of these has been of interest to Atomics International in relevant studies.[4] The last column gives the maximum energy that could be generated in a given volume of the fuel per passage through the critical region. UO_4 could precipitate if this value were exceeded. Since the H_2O_2 solubilities of Table I have been determined at 24°C, the last column of that table is strictly applicable only for that temperature for the fuel as it leaves the critical region. Hence measurements also should be made at higher temperatures as well as with different fuel compositions of interest. Changes in the fuel composition and the temperature might have an important effect on the corrosion of container materials such as titanium, stainless steel, etc.

2. Neutronic Calculations

In connection with the possible application of an aqueous (uranyl sulfate fuel) reactor as a high-flux neutron source, three two-dimensional

Table I

H_2O_2 Solubilities and Corresponding Fission-Pulse Densities
(Temperature, 24°C)

Fuel Composition, molar	H_2O_2 Solubilities, molar	G[a]	Number j/cm^3 pass[b]
0.864 M UO_2SO_4 + 0.50 M H_2SO_4	0.0062 ± 0.004	1.1	54.
0.432 M UO_2SO_4 + 0.50 M H_2SO_4	0.0088 ± 0.004	1.3	65.

[a] G = No. of molecules of H_2O_2 produced per 100 eV of reactor energy. See Ref. 3, Fig. 16.30.

[b] Calculated from No. j/cm^3 pass = (H_2O_2 solubility)/0.000104 G. See Ref. 3, Eq. 16.27.

problems based on one-dimensional survey calculations were run; a system of possible interest (Fig. 1) was then specified. Selected calculational results for this system are presented in Table II. The 2DF (two-dimensional transport) code and the Hansen-Roach 16-group cross-section set[5] (anisotropic hydrogen) were used. Room temperature was assumed for the system.

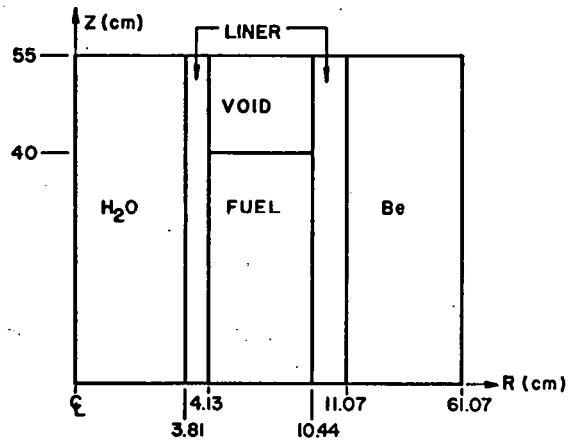

Fig. 1. Geometry of Aqueous Uranyl Sulfate Reactor (Central H_2O Island and Be Reflector).

Table II

Calculated Critical Configuration and Neutron Economy

Material composition:

Fuel:	uranyl sulfate, 1.1 g/ml, 75 g $^{235}U/\ell$, $H/^{235}U$ = 343
Liner:	75 v/o Zr + 25 v/o Ti
Reflector:	Be, 1.8 g/cc

Critical volume (fuel): 11.6 ℓ

Critical mass: 0.87 kg ^{235}U

Maximum centerline fluxes (500 MW):

6.3 x 10^{16} n/cm^2-sec (thermal)

4.5 x 10^{16} n/cm^2-sec (all above thermal)

Neutron economy:

Absorptions:	H_2O	3.55%
	inner liner	1.59
	fuel	57.55
	outer liner	5.12
	Be	3.88
Leakage:	Top	9.4%
	Bottom	16.1
	Side	2.8

II. HIGH TEMPERATURE NEUTRON DETECTOR TEST
(E. O. Swickard, J. L. Bacastow)

A. General

Two high temperature neutron detectors were purchased from each of three manufacturers for evaluation. The detectors have ^{235}U coated electrodes with integral, mineral-insulated cables. Specifications required that both the detector and cable operate at 600°C. The test objective was the determination of the effect of temperature on the following: (1) pulse height distribution; (2) neutron counting sensitivity; (3) detector and cable resistance; (4) detector and cable capacitance; and (5) detector and cable noise.

Detectors with their integral signal cables were installed in four 17-ft high furnaces that contain a helium atmosphere at a few psig. Electrical heaters on the outside of the furnace tube were wired so that those in the detector region and those in the cable region are independently controllable.

The integral cable was connected to a suitable preamp, an amplifier, a scaler, and a 400-channel pulse height analyzer. Counts were taken with and without a neutron source just outside furnace insulation. Measurements were made at ambient temperature, 100, 200, 300, 400, 500, 600, 625, and 650°C.

B. Current Results

All data required by the testing program has been taken; it is currently being analyzed. Figure 2 shows the dependence of leakage current on temperature at constant voltage. Figure 3 is a plot of capacitance vs temperature for 1000 Hz. The effect of temperature on pulse height distribution, neutron sensitivity and noise will be known when analysis of multichannel pulse analyzer data has been completed. Table III shows manufacturer's recommended operating voltage and the maximum voltage that can be used before signal-to-noise ratio becomes unacceptable.

Table III

Detector Identification	Recommended Voltage Range	Maximum Voltage Volts	Maximum Voltage Temp.(°C)	Maximum Voltage at Final Ambient Temp.
W-1	200 - 800	185	600	420
W-2	200 - 800	180	625	255
RS-1	150 - 350	Failed	600	Failed
RS-2	150 - 350	150	625	>350
GE-1	100 - 800	164	650	492
GE-2	100 - 800	172	650	485

All detectors (except RS-1) were held at temperatures of 600°C or above for at least 1000 hours.

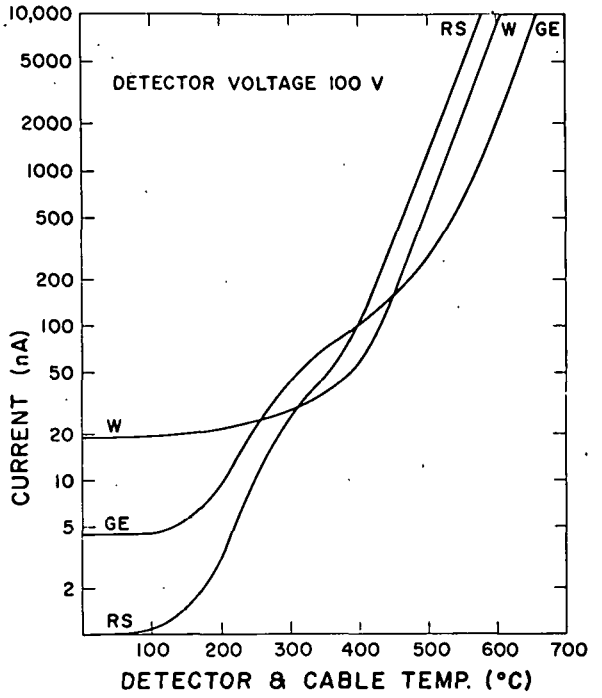

Fig. 2. Variation of Detector Leakage Current at Temperature.

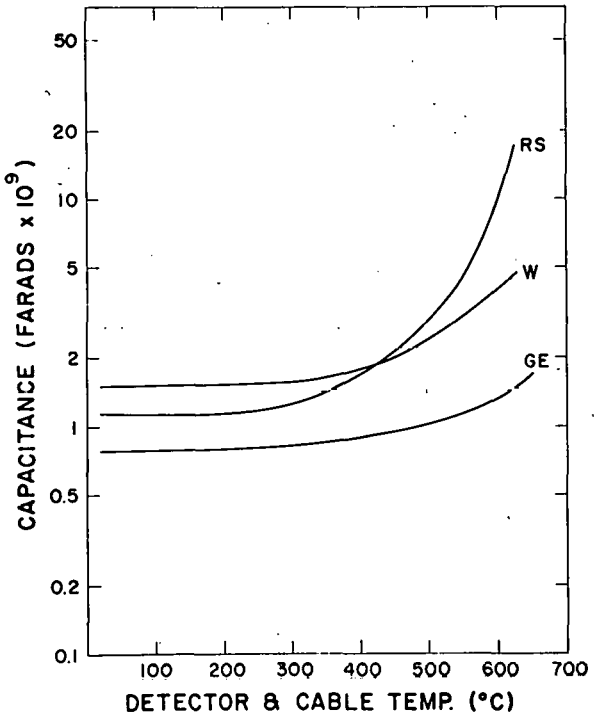

Fig. 3. Variation of Detector Capacitants with Temperature.

III. EQUATION OF STATE OF REACTOR FUELS

(E. O. Swickard, B. Goplen)

A. General

Fast reactor accident analysis requires data on the equation of state for fuel materials at high temperatures. Currently such information is obtained by extrapolation of available low temperature data using an assumed model. Results of such an extrapolation are dependent on the model used and there is little to indicate which model gives correct information.

Shock transient time measurements have been used to calculate the material equation of state for high pressures and low temperatures. By testing material (fuel) of reduced density, this technique may yield data applicable at temperatures and pressures of interest in reactor accident analysis.

A program is underway to investigate the feasibility of (1) fabricating reactor fuel samples with a range of densities down to about one-fourth normal density, and (2) making shock transient time measurements on a series of different density material to find if the method will yield equation of state in the range of interest.

B. Current Results

Small UO_2 samples have been made having densities 10.34, 6.38, and 2.91. These samples have been used in a high explosive experiment which measured shock transient times. The Hugoniot for the material has been calculated. Normalization of the Hugoniot requires the preparation and shooting of much larger samples. Fabrication of the large samples is underway. Data from small sample UO_2 shots is in process of declassification.

Making low density samples of the next material to be tested, UC, is much more difficult than from UO_2. Sample densities less than about 60% of crystalline require porous particles as starting material. Industrial firms are being contacted to find out if porous UC particles are available commercially.

REFERENCES

1. L. D. P. King, Material for the Program Status Report, Weapons Research and Development, Part I, October 1, 1967 to December 31, 1967, Report RFS-480, Los Alamos Scientific Laboratory.

2. M. E. Bunker et al., "Gas Recombination System for the Los Alamos Homogeneous Reactor," Report LA-1337, Los Alamos Scientific Laboratory, 1952.

3. H. F. McDuffie et al., "Aqueous Fuel Systems," p. 363 et seq. in C. R. Tipton, Jr., Reactor Handbook, Vol. I, Materials, Inerscience Publishers, Inc., New York, 1960

4. L. D. P. King, Memorandum RFS-483, Los Alamos Scientific Laboratory, February 2, 1968

5. "Los Alamos Group-Averaged Cross Section," L. D. Connolly, ed., LAMS-2941, Los Alamos Scientific Laboratory (1963).

SPECIAL DISTRIBUTION

Atomic Energy Commission, Washington

Division of Research

D. K. Stevens

Division of Naval Reactors

R. H. Steele

Division of Reactor Development and Technology

Lewis J. Colby
G. W. Cunningham
Donald E. Erb
Nicholas Grossman
Kenneth E. Horton
R. E. Pahler
J. M. Simmons (2)
Edward E. Sinclair
A. Van Echo
C. E. Weber
G. W. Wensch
M. J. Whitman
I. F. Zartman (2)

Division of Space Nuclear Systems

G. K. Dicker
F. C. Schwenk

Idaho Operations Office

DeWitt Moss

Ames Laboratory, ISU

O. N. Carlson
W. L. Larsen
M. Smutz

Argonne National Laboratory

Alfred Amorosi
Frank G. Foote
Sherman Greenberg
J. R. Humphreys
J. H. Kittel
R. E. Macherey
M. V. Nevitt

Idaho Falls, Idaho

D. W. Cissel

Atomics International

R. W. Dickinson, Director
Liquid Metals Information Center

J. L. Ballif

Babcock & Wilcox Co.

C. Baroch
J. H. MacMillan

Battelle Memorial Institute

Donald L. Keller
Stan J. Paprocki

Brookhaven National Laboratory

D. H. Gurinsky
C. Klamut

Combustion Engineering, Inc.

S. Christopher

Donald W. Douglas Laboratories

R. L. Andelin

General Electric Co., Cincinnati, Ohio

V. P. Calkins

General Electric Co., Sunnyvale, Calif.

R. E. Skavdahl

Gulf General Atomic Inc.

E. C. Creutz

Idaho Nuclear Corporation

W. C. Francis

IIT Research Institute

R. Van Tyne

Lawrence Radiation Laboratory

Leo Brewer
J. S. Kane
A. J. Rothman

Mound Laboratory

R. G. Grove

NASA, Lewis Research Center

J. J. Lombardo

Naval Research Laboratory

L. E. Steele

Oak Ridge National Laboratory

G. M. Adamson
J. E. Cunningham
J. H. Frye, Jr.
C. J. McHargue
P. Patriarca
O. Sisman
M. S. Wechsler
J. R. Weir

Pacific Northwest Laboratory

F. W. Albaugh
E. A. Evans

FFTF Project

E. R. Astley
B. M. Johnson
D. W. Shannon (2)

U. S. Department of Interior

Bureau of Mines, Albany, Oregon

H. Kato

United Nuclear Corp.

A. Strasser

Westinghouse, Advanced Reactors Division

W. E. Ray

Westinghouse, Advanced Research Division

E. C. Bishop

Westinghouse, Bettis Atomic Power Laboratory

E. J. Kreigh